Czech Technical University in Prague
Faculty of Electrical Engineering
Department of Electromagnetic Field

Indoor Channel Characterization at the Large and Small Scales

Bachelor thesis

Tomáš Janák

Bachelor programme: Communications, Multimedia and Electronics
Branch of study: Communication technology
Supervisor: Prof. Jeff Frolik

Prague, May 2017

Declaration

I hereby declare I have written this bachelor thesis independently and quoted all the sources of information used in accordance with methodological instructions on ethical principles for writing an academic thesis. Moreover, I state that this thesis has neither been submitted nor accepted for any other degree.

In Prague, May 2017

.....
Tomáš Janák

ČESKÉ VYSOKÉ UČENÍ TECHNICKÉ V PRAZE

ZADÁNÍ BAKALÁŘSKÉ PRÁCE

I. OSOBNÍ A STUDIJNÍ ÚDAJE

Příjmení: **Janák** Jméno: **Tomáš** Osobní číslo: **406507**

Fakulta/ústav: **Fakulta elektrotechnická**

Zadávající katedra/ústav: **Katedra elektromagnetického pole**

Studijní program: **Komunikace, multimédia a elektronika**

Studijní obor: **Komunikační technika**

II. ÚDAJE K BAKALÁŘSKÉ PRÁCI

Název bakalářské práce:

Indoor Channel Characterization at the Large and Small Scales

Název bakalářské práce anglicky:

Indoor Channel Characterization at the Large and Small Scales

Pokyny pro vypracování:

A radio signal´s strength is impacted not only by the distance it travels but also by the environment in which it travels. Of particular interest to modern communication systems is radio propagation in indoor environments. Not only are these environments applicable to current systems (e.g., home WiFi) but to also future Internet of Things (IoT) systems. This thesis project will utilize microwave test equipment (e.g., signal generators, spectrum analyzers, and/or network analyzers) to measure channel loss between a wireless transmitter (T) and receiver (R). The distance between these devices is referred to as the T-R distance. These measurements will be conducted in several indoor settings (e.g., within hallways and office-like environments, and between rooms) and at multiple frequencies considering typical future wireless systems. The measurements will be made to characterize both large- and small-scale propagation effects caused by the environment. To characterize large-scale effects, a transmitter will be fixed in the environment of interest. The receiver will be moved to multiple T-R distances. At each distance, path loss measurements will be made. For each test scenario (environment/frequency) it is expected that approximately 50 measurements will be made and will cover T-R distances form 1 m to 20 m. The data will be used to create a large-scale propagation model (e.g., using log-distance shadowing approach). Small-scale effects will be characterized using three methods to account for spatial, temporal and frequency effects. Using a fixed T-R distance, the receiver will be move short distance to account for spatial variability. To account for temporal variability, the receiver will be fixed but the environment will change (e.g., through motion). To account for frequency variability, the redeiver and environment will be fixed and the frequency will be swept over the band of interest. Data statistics will be captured and compared to well-known fading models (e.g., Rayleigh).

Seznam doporučené literatury:

[1] T. Rappaport, Wireless Communications: Principles and Practice, 2nd Edition, Prentice Hall, 2002.
[2] S.R. Saunders, A. Aragon-Zavala: Antennas and Propagation for Wireless Communication Systems, 2nd Edition, Wiley, 2007.
[3] A. Molisch, Wireless Communications, 2nd Edition, IEEE/Wiley, 2011.

Jméno a pracoviště vedoucí(ho) bakalářské práce:

prof. Jeff Frolik, katedra elektromagnetického pole FEL

Jméno a pracoviště druhé(ho) vedoucí(ho) nebo konzultanta(ky) bakalářské práce:

prof. Ing. Pavel Pechač Ph.D., katedra elektromagnetického pole FEL

Datum zadání bakalářské práce: **14.02.2017** Termín odevzdání bakalářské práce: **26.05.2017**

Platnost zadání bakalářské práce: **25.05.2018**

Podpis vedoucí(ho) práce	Podpis vedoucí(ho) ústavu/katedry	Podpis děkana(ky)

III. PŘEVZETÍ ZADÁNÍ

Student bere na vědomí, že je povinen vypracovat bakalářskou práci samostatně, bez cizí pomoci, s výjimkou poskytnutých konzultací. Seznam použité literatury, jiných pramenů a jmen konzultantů je třeba uvést v bakalářské práci.

Datum převzetí zadání	Podpis studenta

Acknowledgements

I would like to acknowledge and thank the following important people who have supported me, not only during the course of this thesis but throughout all my Bachelor's degree. Firstly, I would like to express my gratitude to my supervisor Prof. Jeff Frolik, for his support and all the advice. I would also like to thank Ing. Pavel Pechač Ph.D. for providing me with all the necessary guidance and insight throughout the research. Special thanks go to Ing. Václav Kabourek for unwavering support during the measurement. Moreover, finally, I would like to thank my family and close friends. You have all encouraged me and supported me.

Abstract

The content of the work is an introduction to radio wave propagation indoors, ways of a simulation and measurement of this propagation. Emphasis is put on the propagation of the waves on super-high or even extremely high-frequency band, considering future deployment of the 5th generation of the mobile network (5G).The thesis contains the theoretical basis of the propagation of the electromagnetic waves, and on this basis, the simulations are implemented. The main part is focused on measurement of fading alongside the radio channel at given frequency band. The measurement is carried out with the available equipment, and the fading statistics is compared with well-known statistical fading models.

Abstrakt

Náplní práce je úvod do šíření rádiových vln uvnitř budov, způsoby simulace a měření tohoto šíření. Důraz je kladen na šíření super krátkých (SKV) nebo dokonce extrémně krátkých vln (EKV) s uvážením budoucího zavádění mobilních systémů 5. generace (5G). Obsahem práce je teoretický rozbor šíření elektromagnetických vln, na jehož základě jsou implementovány simulace. Hlavní částí práce je experimentální měření úniků v rádiovém kanálu v daném frekvenčním pásmu. Měření je prováděno s dostupným vybavením a statistiky úniků jsou porovnány se známými statistickými modely úniků.

Keywords

Radio wave propagation, reflection, refraction, Rayleigh channel, Rice channel, propagation models, physical model, empirical model, fading

Klíčová slova

Šíření rádiových vln, odraz, lom, Rayleighův kanál, Riceův kanál, modely šíření, deterministický model, empirický model

List of Tables

List of Figures

List of Acronyms

CDF Cumulative Distribution Function.

DRH Double Ridge Horn (antenna).

EHF Extremely High Frequency.

IO Interacting Object.

LOS Line Of Sight.

MPC Multi Path Component.

PDF Probability Distribution Function.

RF Radio Frequency.

RX Receiving Antenna.

SHF Super High Frequency.

TX Transmitting Antenna.

VNA Vector Network Analyzer.

Contents

Chapter 1

Introduction

Nowadays, there is a huge demand for wireless communication. To meet consumer demands, the wireless industry is one of the most changing and evolving industry. The performance requirements (connectivity, bandwidth) for the wireless technologies are increasing all the time, and new technologies are needed to satisfy them. One way how to satisfy the bandwidth needs is the deployment of systems working at higher frequencies.

One of the first systems operating in the higher frequency band is WiFi, standard 802.11ac (also called 5G WiFi), works in the 5 GHz band. With the development of the 5th generation of mobile networks (5G), frequency bands assigned to this system are set in a super-high-frequency (SHF) GHz band or even in the extremely-high-frequency (EHF) GHz band. These frequency bands have been explored only limitedly in the past regarding radio wave propagation indoors. This thesis is therefore focused on the propagation in these kinds of environment, in the wide frequency band, particularly in a super high-frequency band, where the 5G WiFi works and the new 5G mobile networks should be working in the future. It is necessary to understand the propagation, its principles to choose the right frequencies and to design reliable communication systems.

The content of the thesis is an introduction to radio wave propagation. Special emphasis is put on the propagation inside buildings and fundamental prediction of this propagation. The main goal of the thesis is corresponding with the requirements for new mobile communication systems and is focused on research of the mechanisms influencing the radio signal, such as distance, frequency, environment, etc. To ensure reliable links, it is needed to know fading statistics for certain scenarios, to set certain fade margin of the system as the system designer. Emphasis is put on how is the fading impacted by the variables mentioned before. Practical goal is to measure certain scenarios for the radio channels and compare measured data to the simulations or the fading statistics from the literature.

Chapter 2

Mechanisms of the propagation

A large number of users of wireless communication systems are located in cities, so there is a demand for knowledge of propagation of electromagnetic waves in an urban environment, especially inside buildings. Let's assume propagation indoors. Description of such propagation is one of the most complicated cases because it depends on various factors such as building materials, distribution of furniture in space, allocation of rooms or surrounding buildings. In some cases, the interior is very complicated and variable in time (opened windows, doors). The electromagnetic energy between transmitter and receiver propagates in many ways – direct propagation, transmission through the walls or furniture, diffraction, reflection from walls and other mechanisms.

2.1 Free space loss

The simplest possible scenario is a propagation of a spherical wave from a point of source in free space. The power density at distance d from the isotropic transmitter (TX) antenna is $P_{TX}/(4\pi d^2)$. Now we assume a receive (RX) antenna in distance d with the gain G_{TX} and 'effective' area A_{RX}. We can suppose that all transmitted power is collected by the RX antenna, then the received power is as follows [1]:

$$P_{RX}(d) = P_{TX}\frac{1}{4\pi d^2}A_{RX} \tag{2.1}$$

In the case of the non-isotropic antenna, the formula has to be multiplied with antenna gain G_{TX} in the direction of the receiver (RX) antenna. In general, we can show the relationship between antenna gain and effective area A [1]:

$$G = (\frac{4\pi}{\lambda^2})A \tag{2.2}$$

As we can see, for the fixed antenna area, the gain increases with the frequency. Now the received power in free space can be expressed as a function of distance d [1]:

$$P_{RX}(d) = P_{TX}G_{TX}G_{RX}(\frac{\lambda}{4\pi d})^2 \tag{2.3}$$

We can get well known equation - Friis' law [1]:

$$\frac{P_{RX}}{P_{TX}} = G_{TX}G_{RX}(\frac{\lambda}{4\pi d})^2 \tag{2.4}$$

The fraction $(4\pi d/\lambda)^2$ is also known as *free space loss factor*. In many cases, it is advantageous to transfer Friis' law on logarithmic scale [1]:

$$P_{RX} = P_{TX} + G_{TX} + G_{RX} + 20\ \log(\frac{\lambda}{4\pi d}) \tag{2.5}$$

where P_{TX},P_{RX} are in units of dBm and G_{RX},G_{TX} are in dB. Free space loss factor L_{FSL} expressed in dB [2]:

$$L_{FSL} = 20\log(\frac{\lambda}{4\pi d}) \tag{2.6}$$

can be expressed in useful units as well [2]:

$$L_{FSL} = 32.4 + 20\ \log(f_{MHz}) + 20\ \log(d_{km}) \tag{2.7}$$

where f_{MHz} is frequency in MHz and d_{km} is distance in kilometers. Received power is then decreasing with the second power of distance.

2.2 Reflection, Refraction and Transmission

Assume the geometry as in Fig. 2.1, plane wave incidents onto an infinitely large plane boundary between two lossless media with different material constants μ_1, ϵ_1, σ_1 and μ_2, ϵ_2, σ_2. The incident wave makes an angle θ_i to the normal. Under these assumptions, reflection and refraction happen on the surface. The solution of Maxwell's equations dictates that at the point of impact two new waves are produced, transmitted and reflected, both with the same frequency as the incident wave. For both waves, their Poynting vector lies in the plane which contains both the incident wave and the normal to the surface; this is the scattering plane. The first wave reflected from the surface stays in the first medium, makes an angle θ_r to the normal of interface and is called the *reflected wave*. The second wave travels into the other medium, making an angle with the normal interface θ_t and is known as a *transmitted wave*.

Thus, the following condition holds $\mathbf{E} \perp \mathbf{H} \perp \mathbf{k}$.

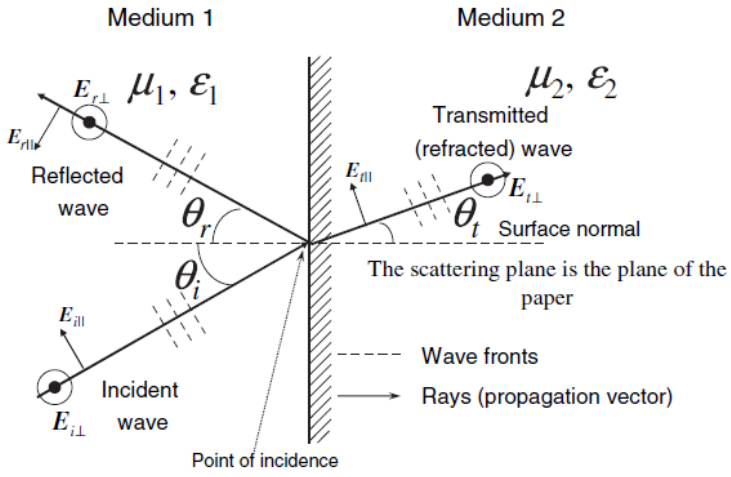

Figure 2.1: Reflection of the plane wave [3]

The angle of the reflected and transmitted wave is related to the incident wave as follows:

$$\theta_i = \theta_r \tag{2.8}$$

$$\frac{sin\,\theta_t}{sin\,\theta_i} = \frac{k_1}{k_2} \tag{2.9}$$

where k_1 a k_2 are propagation constants for medium 1 and medium 2. Equations 2.8 a 2.9 are expressing Snell law of reflection and refraction. Change of phase velocity is expressed as the refractive index n, which can be expressed by free space phase velocity and phase velocity in a medium as:

$$n = \frac{c}{v} = \frac{ck}{\omega} \tag{2.10}$$

so we can express Snell's law for permeabilities μ_1=μ_2 as:

$$\frac{sin\,\theta_t}{sin\,\theta_i} = \frac{k_1}{k_2} = \frac{n_1}{n_2} = \frac{Z_2}{Z_1} \tag{2.11}$$

where n is an index of refraction, v is phase velocity in medium, k is wave number, ω is radial frequency and Z is wave impedance of the mediums.

In addition to the change of direction of the wave, there is a distribution of incident wave energy between transmitted and reflected wave on the surface boundary. The amplitudes of the reflected and transmitted waves are given relative to the amplitude of the incident wave by using reflection coefficient R and transmission coefficient T. Coefficients are different for the case, when electric field $\mathbf{E}$ is normal to the scattering plane, and for the case when electric field $\mathbf{E}$ is parallel to the scattering plane.

The coefficients depends on the angles and on the impedances:

$$R_{\perp} = \frac{E_r}{E_i} = \frac{Z_2\, cos\theta_i - Z_1\, cos\theta_t}{Z_2\, cos\theta_i + Z_1\, cos\theta_t} = \frac{Z_2\, cos\theta_i - Z_1\sqrt{1 - (\frac{Z_2}{Z_1})^2\, \sin^2\theta_i}}{Z_2\, cos\theta_i + Z_1\sqrt{1 - (\frac{Z_2}{Z_1})^2\, \sin^2\theta_i}} \tag{2.12}$$

$$T_{\perp} = \frac{E_t}{E_i} = \frac{2Z_2 \cos\theta_i}{Z_2\, cos\theta_i + Z_1\, cos\theta_t} = \frac{2Z_2 \cos\theta_i}{Z_2\, cos\theta_i + Z_1\sqrt{1 - (\frac{Z_2}{Z_1})^2\, \sin^2\theta_i}} \tag{2.13}$$

$$R_{\parallel} = \frac{E_r}{E_i} = \frac{-Z_1\, cos\theta_i + Z_2\, cos\theta_t}{Z_2\, cos\theta_t + Z_1\, cos\theta_i} = \frac{-Z_1\, cos\theta_i + Z_2\sqrt{1 - (\frac{Z_2}{Z_1})^2\, \sin^2\theta_i}}{Z_1\, cos\theta_i + Z_2\sqrt{1 - (\frac{Z_2}{Z_1})^2\, \sin^2\theta_i}} \tag{2.14}$$

$$T_{\parallel} = \frac{E_t}{E_i} = \frac{2Z_2 \cos\theta_i}{Z_2\, cos\theta_t + Z_1\, cos\theta_i} = \frac{2Z_2 \cos\theta_i}{Z_1\, cos\theta_i + Z_2\sqrt{1 - (\frac{Z_2}{Z_1})^2\, \sin^2\theta_i}} \tag{2.15}$$

Previous equations are expressed in terms of θ_i, to avoid calculating θ_t; for dielectric mediums where permitivities of the mediums $\sigma_1 = \sigma_2 = 0$ and permeabilities $\mu_1 = \mu_2$.
In the case of conductive surface and small angles of impact, which is the case of the wave reflection from the ground in most terrestrial links, reflection coefficient can be generalized for both polarizations as follows:

$$R \approx 1e^{j\pi} = -1 \tag{2.16}$$

We can also derive useful relations, which consider the law of the energy conservation at the point of impact - since the energy of the incident wave is divided between both waves following equations applies:

$$|T_{\perp}|^2 = 1 - |R_{\perp}|^2 \tag{2.17}$$

$$|T_{\parallel}|^2 = 1 - |R_{\parallel}|^2 \tag{2.18}$$

2.3 Waveguiding

According to [2], process of waveguiding models propagation in corridors, street canyons, and tunnels. However, these situations are very complicated, difficult to predict and deviate from idealized waveguides in the following ways:

- the materials are lossy
- corridors do not have continuous walls, but are interrupted at more or less regular intervals by windows, doors, etc.
- street canyons, furthermore, do not have the 'upper' wall of the waveguide
- the surfaces are rough
- the 'waveguides' are not empty, but filled with interactive objects (people, cars, etc.)

A geometric optics approximation can be used to predict specific propagation in waveguide-like environment. Computing the waveguide modes would be different approach of prediction.
Conventional theory assumes a propagation loss in the waveguides that increases exponentially with distance. The majority of measurements concludes the propagation follows d^{-n} law, where n varies from 1,5 to 5. If energy is guided, even d^0 becomes theoretically possible.

2.4 Multipath propagation

Interactions of the electromagnetic wave with the interacting objects (IOs) cause mechanism called *multipath propagation*, where the signal from the TX can get to RX via a large number of different paths. There can be infinite number of these propagation paths and each of them has a different amplitude, time delay, direction of departure from TX (known as Angle Of Arrival), direction of arrival to RX (known as Angle Of Departure) and, most importantly, different phase shifts with respect to each other. The multipath propagation can be described with geometric optics, where the propagation paths are modeled as rays. In the point of receive, the electric fields of the rays are summed up:

$$\mathbf{E} = \sum_i \mathbf{E}_i \tag{2.19}$$

where $\boldsymbol{E}$ is total electric field.

2.5 Fading

The different Multi Path Components (MPCs) are added up in the simple RX. They interfere with each other, either constructively or destructively, depending on the MPC's phases as shown in Fig. 2.2. Moreover, the phases mostly depend on propagation time of the MPC, thus on the position of the mobile station and the IO's. If either TX, RX or IOs are changing their positions even slightly, it affects the interference, thus it affects the amplitude of the total signal. This changing of the amplitude is called *small-scale fading*.

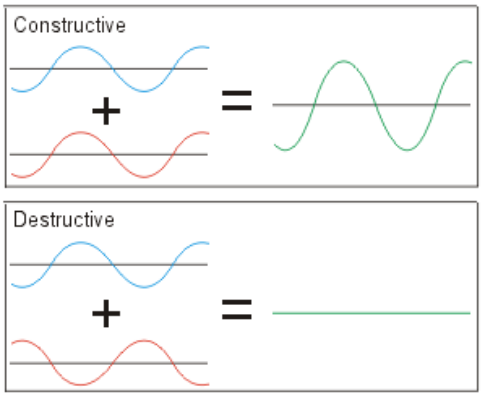

Figure 2.2: Constructive and destructive interference

Also, each MPC's amplitude can change with time or location. Obstacles can cause such situation, when *shadowing* occurs. The RX moves behind the large obstacle and amplitude of this component that propagates between TX and RX significantly decreases because RX is in the radio shadow and any wave going through the obstacle is greatly attenuated. The RX has to move over a large distance to get out radio shadow that is why we are talking about *large-scale fading*.

Another way we can describe large-scale and small-scale fading is using typical plot depicting received power as a function of distance. As we can see in the insert in Fig. 2.3, power fluctuates around a local mean value on a short-distance scale. These fluctuations are caused by the interference of different MPCs as it was mentioned before in this chapter and are called *small-scale fading*.

When we take a look at the larger scale, about hundreds of wavelengths, we can see that mean received power shows fluctuations as well. It can be seen most clearly when moving in a circle around the transmitter, shown in Fig. 2.4. The reason for this *large-scale fading* is shadowing by the Interacting Objects IOs, and its mean monotonically depends on the distance between transmitter and receiver. The large scale mean also depends on the distance between RX and TX, the mean decreases as the consequence of the free space loss described in Section 2.1.

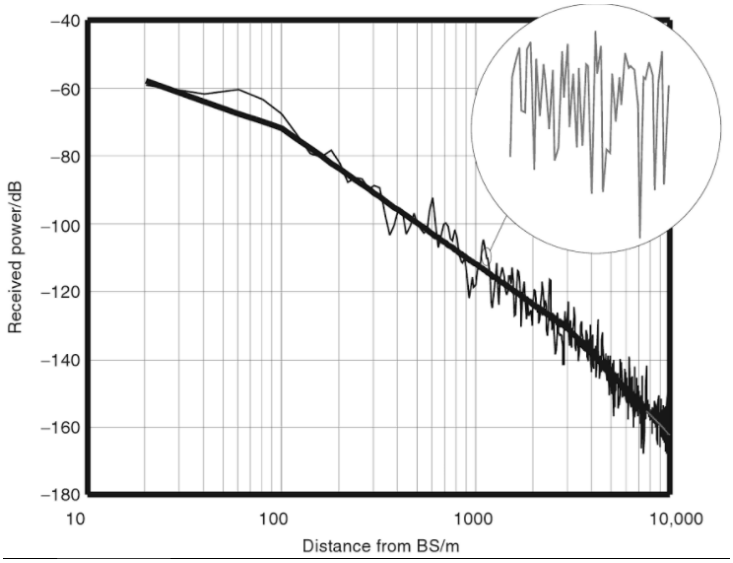

Figure 2.3: Received power as a function of distance from the TX [1]

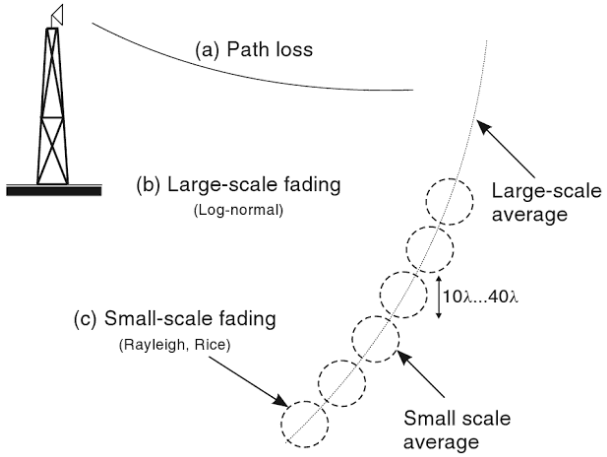

Figure 2.4: Various fluctuations of received power [1]

It is almost impossible to predict the received signal due to the fading. Therefore, statistical descriptions are used to determine the mean amplitude of the received signal and fluctuations around the mean value.

Chapter 3

Statistical description of the wireless channel

As there are many reflection, diffraction and scattering processes in the radio channel, it is complicated to describe the different MPCs. We can only set a probability that certain parameter attains certain value. It can be done by a series of longterm measurement of these parameters. By these measurements we get the *probability density function* (*PDF*), which shows the probability of the individual parameter values. More useful can be the *cumulative density function* (CDF), which defines the probability, that the certain variable has a value smaller than x. Therefore the *cdf(x)* is defined as the integral of the *pdf*:

$$cdf(x) = \int_{-\infty}^{x} pdf(u)du \tag{3.1}$$

It is convenient to compare fading statistics with well known distributions. The most popular are Gauss distribution, log-normal distribution, Rayleigh distribution, Rice distribution, etc.

Typically, the large scale fading have log-normal distribution, on the other hand, small scale fading have Rayleigh or Rice distribution. For our purposes we will further describe Rayleigh and Rice fading in the subsequent text.

3.1 Rayleigh distribution

Consider a scenario of propagation without dominant LOS component, where N homogeneous plane waves (MPCs) have been created by reflection/scattering from several IOs. We consider radio channel where IOs and TX do not move and RX moves with a velocity v. Moreover, we assume that the absolute amplitudes of the MPCs are constant over all region of observation.
The total fieldstrength in terms of in-phase and quadrature-phase components in real passband notation [1]:

$$E_{BP}(t) = \sum_{i=1}^{N} I(t) \cdot cos(2\pi f_c t) - Q(t) \cdot sin(2\pi f_c t) \tag{3.2}$$

where both in-phase and the quadrature component are the sum of many random variables, which none is dominant. Central limit theorem says that the PDF of such a sum is a normal Gaussian distribution. The *pdf* of the the zero-mean Gaussian distribution with the variance σ^2 [1]:

$$pdf_x(x) = \frac{1}{\sqrt{2\pi}\sigma} e^{-\frac{x^2}{2\sigma^2}} \tag{3.3}$$

The previous formulas are stated in statistics of real and imaginary parts, [1] derives the statistics of amplitude and phase of the received signal.The *pdf* is a product of a *pdf* for ψ - namely, a uniform distribution:

$$pdf_\psi(\psi) = \frac{1}{2\pi} \tag{3.4}$$

and for r - namely, a Rayleigh distribution:

$$pdf_r(r) = \frac{r}{\sigma^2} e^{-\frac{r^2}{2\sigma^2}} \qquad 0 \leq r < \infty \tag{3.5}$$

For $r < 0$ the *pdf* is zero, as amplitudes are by definition positive. Basic properties of the Rayleigh distribution are shown in Table 3.1:

	Rayleigh distribution
Mean value	$\overline{r} = \sigma\sqrt{\frac{\pi}{2}}$
Mean square value	$\overline{r^2} = 2\sigma^2$
Variance	$\overline{r^2} - \overline{r}^2 = 2\sigma^2 - \sigma^2\frac{\pi}{2} = 0,429\sigma^2$
Median value	$r_0 = \sigma\sqrt{2 \cdot ln2}$

Table 3.1: Properties of the Rayleigh distribution [2]

Cumulative distribution function CDF, *cdf(r)* of the Rayleigh distribution is integral of its pdf:

$$cdf(r) = 1 - e^{-\frac{r^2}{2\sigma^2}} \tag{3.6}$$

For small values of r we can use approximation for this:

$$cdf(r) \approx \frac{r^2}{2\sigma^2} \tag{3.7}$$

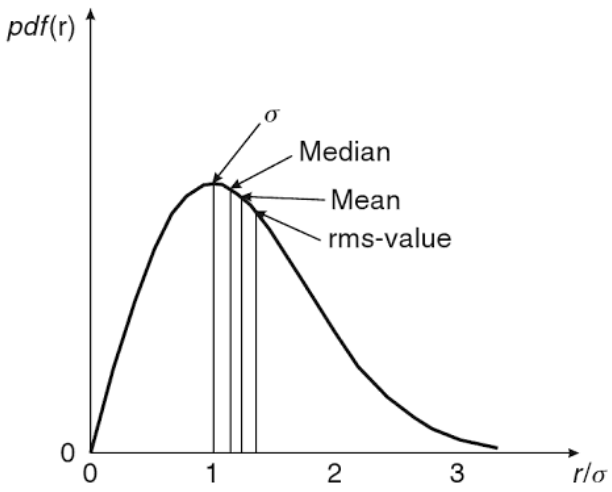

(a) Probability distribution function [1]

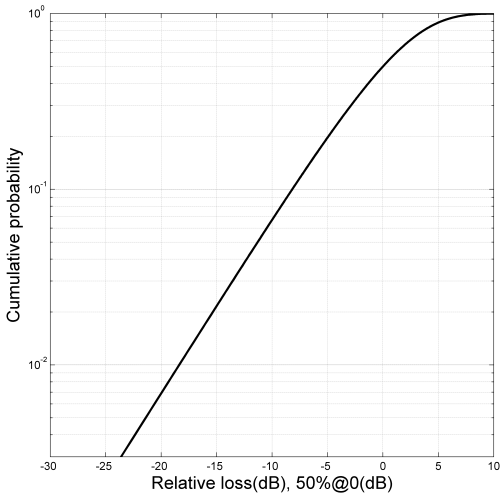

(b) Cumulative distribution function

Figure 3.1: Rayleigh distribution

In Fig. 3.1b, the CDF of the Rayleigh distribution is presented. We will compare all our small scale effects to this CDF. For the no-fading case (constant signal strength over small-scales in time, frequency, and position), the curve is a unit step occurring at 0 dB. Between the non-fading and Rayleigh scenarios, the more severe the fading, the greater the clockwise rotation of the CDF curve about the crossover point. The CDF curve enables to set link fade margins base on an allowable outage probability as well. For example, in Fig. 3.1b, when we want to achieve the outage probability less than 2%, the fade margin needs to be at least 15 dB (relative to the median - 0 dB). Utilizing the proper fading model allows system designers to properly balance transmission power and availability requirements [4].

3.2 Rice distribution

In case we have a dominant MPC like a LOS component, fading statistics change. Consider that LOS component has zero phase, it means the phase is purely real. Therefore, the real part has non-zero-mean Gaussian distributions and imaginary part has a zero-mean Gaussian distribution. We have the joint *pdf* of amplitude r and phase ψ [1]:

$$pdf_{r,\psi}(r,\psi) = \frac{r}{2\pi\sigma^2} e^{-\frac{r^2+A^2-2rAcos(\psi)}{2\sigma^2}} \tag{3.8}$$

where A is the amplitude of the dominant component.
Rice distribution defines the *pdf(r)* of the amplitude as follows:

$$pdf_r(r) = \frac{r}{\sigma^2} \cdot e^{-\frac{r^2+A^2}{2\sigma^2} \cdot I_0(\frac{rA}{\sigma^2})} \qquad 0 \leq r < \infty \tag{3.9}$$

where $I_0(x)$ is the modified Bessel function of the first kind, zero order.

In Fig. 3.2, the PDF of the Rice distribution for three values of the Rice factor K_r. Rice factor is the ratio of the power in the LOS component A to the deviance of the multipath [1]:

$$K_r = \frac{A^2}{2\sigma^2} \tag{3.10}$$

The stronger the LOS component, fades become relatively less deep. For $K_r \to 0$, the Rician distribution degenerates to a Rayleigh distribution. In Fig. 3.3, there is the CDF for five different Rice factor again, as the integral of the PDF (3.2).

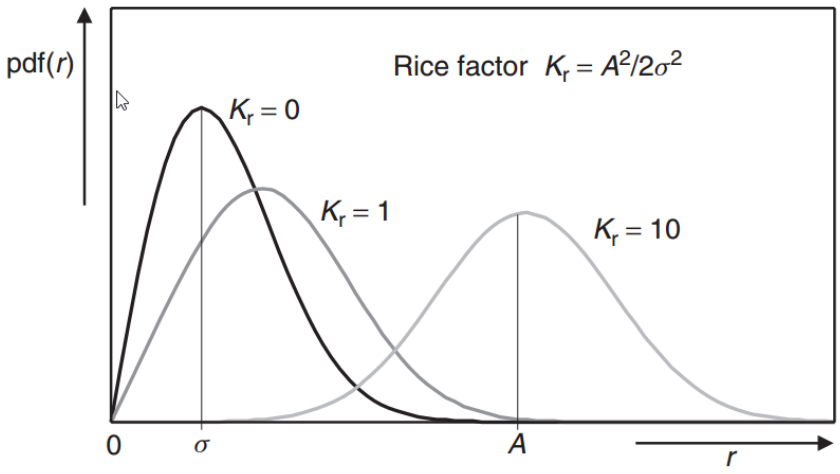

Figure 3.2: Rice distribution - Probability distribution function [1]

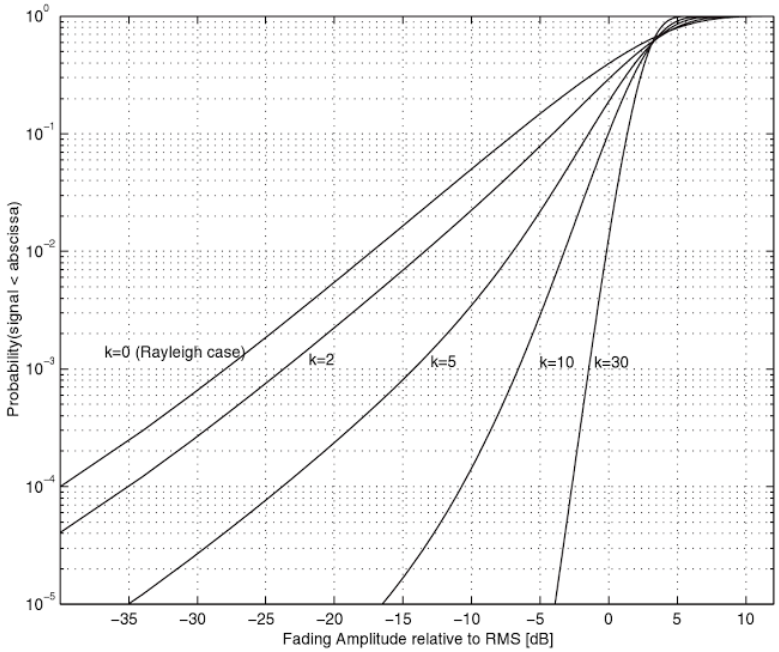

Figure 3.3: Rice distribution - Cumulative distribution function [1]

As far as the further text is concerned, the key things from this chapter would be the CDF of Rayleigh distribution which will be used to compare measured data to Rayleigh distribution. In case the data are similar to Rician distribution, the Rice factor will be calculated.

Chapter 4

Propagation models

Radio wave propagation in an uncertain random environment can be described by so-called propagation models, which provide more or less satisfactory results in comparison with the real situation. The common characteristic of those models is a sort of compromise between the complexity of the calculations and the requirements for a particular model. In this chapter the classification of these models is presented, as well as the theoretical background of the most known models. As part of the thesis, two propagation models were implemented, the outputs of the implementation are presented in the chapter as well.

4.1 Classification

The classification depends on the nature of the calculations respectively the quality of the output data. The character of the calculation often causes different computing and time demands of a particular model. Based on these properties, the models can be distinguished as follows:

- **Physical models** are directly based on the theory of propagation of electromagnetic waves and are complex methods based on the solution of the wave equation
- **Empirical models** use statistical analysis of large amounts of data acquired experimentally for a specific case. These models do not take into account the theoretical principles of electromagnetic wave propagation
- **Semi-deterministic models** are the combinations of the previous two types of models

4.2 Physical models

Physical models, based on the physical nature of electromagnetic wave propagation, are used as a universal means to predict the propagation in urban areas especially when simpler empirical or semi-empirical models do not give satisfactory results.

Most common models are optical models based on geometric optics. In this case, electromagnetic waves are represented as individual rays, with the condition that the dimensions of the objects are significantly larger than the wavelength of the wave. This assumption is for the typical dimensions of the buildings and the high-frequency band more or less fulfilled [2].

In the case of propagation of radio waves along a corridor with a direct line of sight, in addition to the direct ray, the rays reflected from the floor, the side walls and from the ceiling appear. An infinite number of rays exist between two points of space. However, due to multiple reflections or refractions, the wave carries only a small portion of the original energy after the finite number of these reflections (refractions). It is possible to limit the number of reflections, refractions, and transmissions of the electromagnetic wave for the purpose of the calculation. In the point of reception, individual rays are added up regarding complex and vector adding. The calculation can be formally split into two parts. The first part we can call a geometric part and the other one we can call the electromagnetic part.

The geometric part of the calculation is based on finding all relevant rays (paths, in which the wave propagates) between the two antennas of a radio link. We can say these rays carry a considerable part of the energy. At the same time, the rays with more than the limit number of reflections (usually 5 to 6), diffraction or transmissions are omitted. This omission is related to the fact that each reflection, diffraction or passage means a loss of energy.

There are two ways of finding the significant rays:

- Ray tracing – the method using the mirroring to watch the rays between the transmitter and receiver antenna

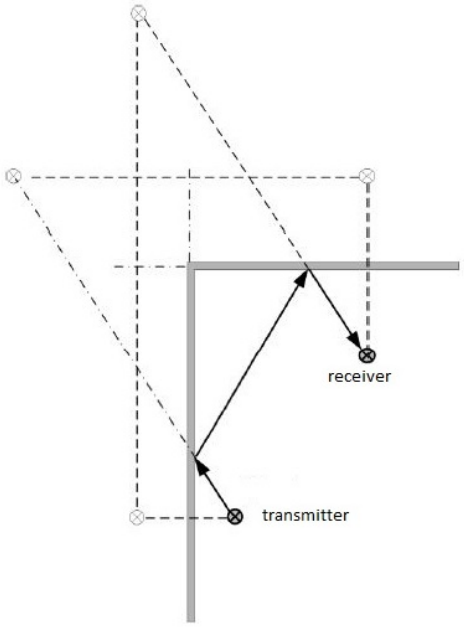

Figure 4.1: Principle of ray tracing [2]

- Ray launching – this way of finding significant rays is based on antenna, transmitting the test rays in several discrete angles. These rays interact with obstacles in the environment in which they travel. The new secondary source of rays is created at the point of impact on an obstacle. Finally, the total sum of the received power includes only those rays that hit the defined volume around the point of reception.

In the electromagnetic part, the individual contributions of significant rays found in geometric part of calculation are enumerated and added up together. In general, it is a complex sum of vectors:

$$\sum \mathbf{E} = \sum_i \mathbf{E}_i \tag{4.1}$$

where $\boldsymbol{E}$ is an electric field in point of receive, $\boldsymbol{E}_i$ is an electric field of i^{th} contribution.

Contribution to the total electric field in point of reception [2] :

$$\mathbf{E}_i = \mathbf{E}_0 F(\vartheta, \varphi) \frac{e^{-jkd}}{d} \prod_{m=1}^{M} R_m \prod_{n=1}^{N} D_n \prod_{q=1}^{Q} P_q \tag{4.2}$$

where $\boldsymbol{E}_0$ represents reference field (V/m), ϑ and φ are spherical coordinates, defining direction of ray propagation from a transmitter, F (ϑ, φ) is normalized radiation amplitude pattern (-), d is the total trajectory of ray (m), $k = 2\pi/\lambda$ is wavenumber (m^{-1}), M is total number of reflections, N is total number of refractions, Q is total number of transmissions on the ray path (-), $\boldsymbol{R}_m$ is coefficient of m^{th} reflection (-), $\boldsymbol{D}_n$ is coefficient of n^{th} refraction (-), $\boldsymbol{P}_q$ is coefficient of q^{th} transmission (-).
From the preceding, the distinct mechanisms of the propagation of electromagnetic waves, are, therefore, processed separately in the calculation.

4.3 Empirical models

Empirical models use statistical analysis of experimental data set to predict radio wave propagation. These models do not take into account theoretical principles of the propagation, thus the model is not versatile. For example, empirical model implemented for an outdoor environment cannot be used indoors or vice versa.

4.3.1 Basic empirical model

Path loss is directly given by the n^{th} power of distance; thus, this is the most common method of predicting the signal coverage in urban canyons. The model is characterized by a very quick and easy calculation. The received power, in this case, is calculated as follows:

$$P_p \approx \frac{1}{d^n} \tag{4.3}$$

where d is the distance from transmitter and n is path loss exponent, which shows how fast is the loss increase with distance. Loss L in decibels is given by:

$$L(d) = L_1(d_1) + 10n \log(\frac{d}{d_1}) \tag{4.4}$$

where d_1 is reference distance (unit), L_1 is reference loss at reference distance d_1 (dB), d is the distance from the transmitter (m), L is path loss (dB); typical values of the exponent are shown in Table 4.1:

Medium	n[-]
free space loss	2.0
suburban area	2.5 to 4.0
dense urban area	3.0 to 5.0
indoors – line of sight	1.6 to 1.8
indoors – non-line of sight	3.0 to 6.0

Table 4.1: Typical values of path loss exponent [2]

Reference loss can be calculated based on the formula for free space loss:

$$L_1 = 20 \log(\frac{4\pi d}{\lambda}) \tag{4.5}$$

Path loss in an empirical model is a function of single variable - distance. This model, therefore, does not respect the specific geometry of the link. Because of this, the model is employable in a more or less homogeneous environment, and its accuracy depends on the experimental parameters obtained during the measurement.

Implementation of the basic empirical model in picocells is called One-Slope model [5]. This model is suitable for fast prediction of propagation indoors, but the results obtained by this model have to be considered only as approximate and indicative. The calculation is almost the same as for the basic empirical model, but the distance d must be smaller than the distance of the Fresnel zone break point. This condition is for common interiors almost always satisfied. The formula for predicted path loss L distance d is as follows:

$$L(d) = L_1 + 10n \log(d) \tag{4.6}$$

where *L(d)* represents predicted path loss (dB), d is the distance between the transmitter and point of observation (m), L_1 is reference path loss for distance 1 m (dB), n is path loss coefficient (-).
Values of parameters L_1 and n for One-slope model and various frequencies are shown in Table 4.2.

f [GHz]	Environment	L_1[dB]	n[-]
1.8	Office area	33.3	4.0
1.8	Free space	37.5	2.0
1.8	Corridor	39.2	1.4
1.9	Office area	38.0	4.0
1.9	Free space	38.0	2.1
1.9	Corridor	38.0	1.3
2.5	Office area	38.0	4.2
2.5	Corridor	38.0	1.2
2.5	Office area	40.0	3.5
2.5	Office area	40.0	3.7
5.0	Office area	46.4	3.5
5.3	Office area	46.8	4.6

Table 4.2: Parameters for One-slope model[1]

4.3.2 Model ITU-R P.1238

This model standardized by ITU is based on the same principle as One-Slope model, except that the reference attenuation is expressed in a different way, a different classification of the interiors is implemented and the calculation includes the propagation between floors. The mean value of the attenuation of the wave propagation, in picocell for distances before the Fresnel zone breakpoint, is given by [5]:

$$L(d) = 20\log(f) + 10n\log(d) + L_f(k_f) - 28 \tag{4.7}$$

where L(d) is a predicted path loss (dB), f is a frequency (MHz), n is a path loss exponent (-), d is a distance between the transmitter and the observation point (m), L_f is a floor penetration loss (dB), k_f is a number of penetrated floors (-).

4.3.3 Dual slope model

It is another model based on the basic empirical model, but with the consideration of Fresnel zone break point. It means, path loss exponent has a different value for distances before and after the breakpoint. This model is designed for microcells or larger picocells in direct line of sight between the two ends of the link. As mentioned above, it is a basic empirical model with two different path loss exponents:

$$L(d) = L_1 + 10n_1\log d, d \leq d_0 \tag{4.8}$$

$$L(d) = L_1 + 10n_1\log(d_0) + 10n_2\log(\frac{d}{d_0}), d \geq d_0 \tag{4.9}$$

where L(d) is predicted path loss (dB), L_1 is a reference path loss in 1 m distance (dB), d is a distance between the transmitter and the observation point (m), n_1 is a path loss exponent for $d \leq d_0$ (-), n_2 is a path loss exponent for $d \geq d_0$ (-), d_0 is a breakpoint, typically distance of a Fresnel zone breakpoint (-):

$$d_0 = \frac{4h_1h_2}{\lambda} \tag{4.10}$$

where h_1, h_2 are antenna heights (m) and λ is a wavelength (m). Typical values of path loss exponent are $n_1 = 2$ and $n_2 = 4$, but usually are these values calibrated based on measured data.

4.4 Implementation of the models

In the previous text, the theoretical analysis of the propagation of electromagnetic waves was given, especially inside buildings along the long corridors. A comparison of the several models for predicting the propagation along the corridor was given as well. The acquired knowledge is practically used in the simulations where two selected models of electromagnetic wave propagation are implemented. In this case, we have selected two models - one empirical and one physical. The aim of this chapter is a practical implementation of the models for the case of a long corridor in the SHF band. Frequency range is set from 5 GHz to 30 GHz. In the selected frequency range only a few representative frequencies are chosen for the simplicity and brevity. The implemented models are further used for comparison with experimentally measured data. All scripts are made in MATLAB.

4.4.1 Physical model

The most common type of the deterministic model is an optical model. Because this model respects the geometric situation, it is needed to define the environment in which the electromagnetic wave considered in the simulation propagates. Let's assume a long hallway with the dimensions given in Fig. 4.2. The length of the corridor was established at 100 m.

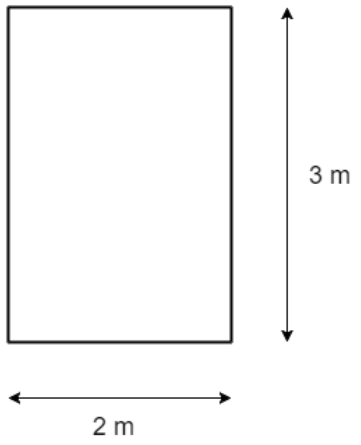

Figure 4.2: Cross-sectional dimensions of the corridor

The calculation of the electric field of the i^{th} ray path is based on the Equation 4.2 which was introduced in Section 4.2. In our case, this equation is considerably simplified, since we are considering only one reflection, no refraction, and no penetration. Further simplification is based on considering with only the main beam which is also infinitely narrow, therefore is F $(\vartheta, \phi) = 1$. When we make all these simplifications, the complex electric field $\boldsymbol{E}_i$ associated with the i^{th} ray path is determined by:

$$\mathbf{E}_i = \mathbf{E}_0 \frac{e^{-jkd}}{d} \mathbf{R} \tag{4.11}$$

where $\boldsymbol{R}$ is the reflection coefficient (-), d is the total trajectory of a ray (m), $k = 2\pi/\lambda$ is the wavenumber (m^{-1}), E_0 is a reference field (V/m), in our case:

$$\mathbf{E}_0 = \sqrt{60 \cdot P_{TX} \cdot G_{TX}} \tag{4.12}$$

where P_{TX} is a power of the transmitter (W), G_{TX} is a gain of transmitter (-).
A reflection coefficient is a complex number, but, according to [1] as the incident angle is very small and for the surfaces with high conductivity can be the reflection coefficient put as $\boldsymbol{R}$ = -1. This value of $\boldsymbol{R}$ is used for all reflections in our simulation.
The used settings are as follows: transmit power is 1 Watt, transmit antenna gain is 0 dBi (ratio equal to one), the height of the transmitter and receiver is 1 m, frequency range 5 GHz to 30 GHz, sampling spacing is 1 mm. Sampling distance is chosen so that it would be smaller than the wavelength of the highest frequency, therefore lower than the wavelength for 30 GHz, which is calculated as 1 centimeter.

With one reflection considered, there is a 5-ray model for our corridor with these significant rays:

- direct ray
- ray reflected from the floor
- ray reflected from the wall 1
- ray reflected from the wall 2
- ray reflected from the ceiling

To find these rays, a simple ray-tracing has been implemented, which includes calculation of the trajectory between the transmitter and receiver antenna. Finding of the reflected rays is graphically illustrated in Figs. 4.3 and 4.4.
Trajectories of the significant rays can be easily expressed as relationship for the distance of two points in space, with coordinates $[a_1, a_2, a_3]$ and $[b_1, b_2, b_3]$:

$$d = \sqrt{(b_1 - a_1)^2 + (b_2 - a_2)^2 + (b_3 - a_3)^2} \tag{4.13}$$

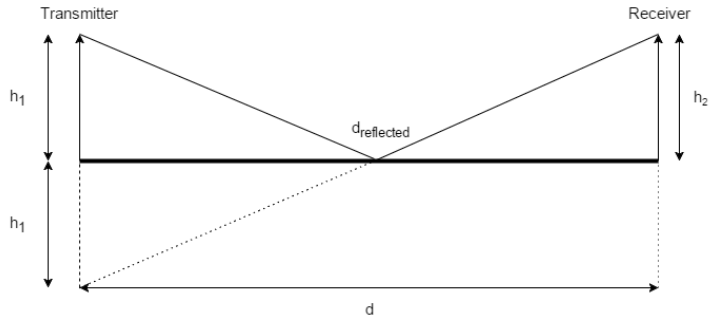

Figure 4.3: Propagation of the reflected wave

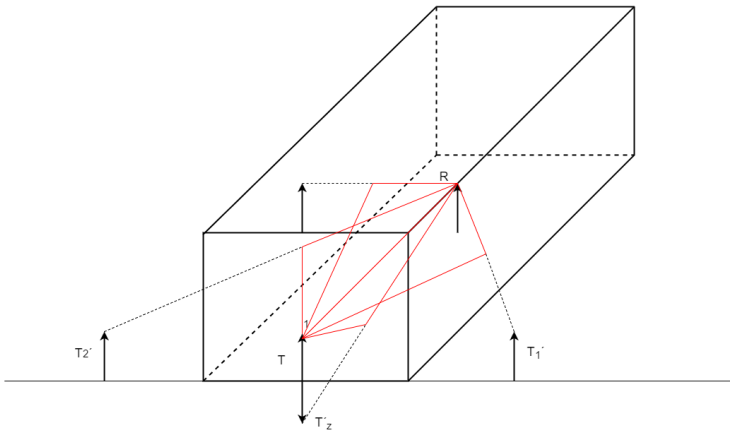

Figure 4.4: Propagation of the significant rays in the corridor

Total phasor of the electric field is, therefore:

$$\mathbf{E} = \mathbf{E}_0\left(\frac{e^{-jkd_{dir}}}{d_{dir}} + R_f\frac{e^{-jkd_f}}{d_f} + R_{w1}\frac{e^{-jkd_{w1}}}{d_{w1}} + R_{w2}\frac{e^{-jkd_{w2}}}{d_{w2}} + R_{ceil}\frac{e^{-jkd_{ceil}}}{d_{ceil}}\right) \tag{4.14}$$

where d_{dir} is the trajectory of the direct ray, d_f is the trajectory of the ray reflected from the floor, d_{w1} is trajectory of the ray reflected from the wall 1, d_{w2} is trajectory of the ray reflected from the wall 2, d_{ceil} is the trajectory of the ray reflected from the ceiling, R_f is the reflection coefficient for the floor, R_{w1} is the reflection coefficient for the wall 1, R_{w2} is the reflection coefficient for the wall 2, R_{ceil} is the reflection coefficient for the ceiling. The following Figs. illustrate how the amplitude of phasor of the electric field depends on the distance from the transmitter for different frequencies:

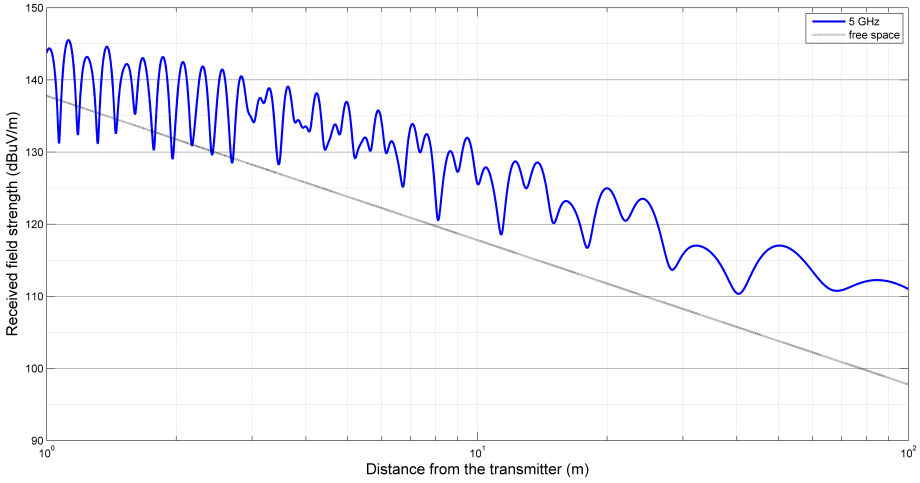

(a) 5 GHz

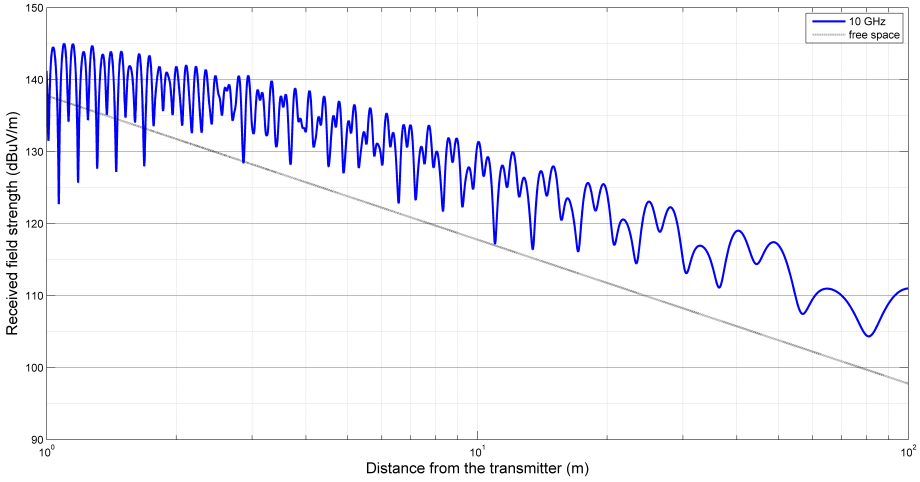

(b) 10 GHz

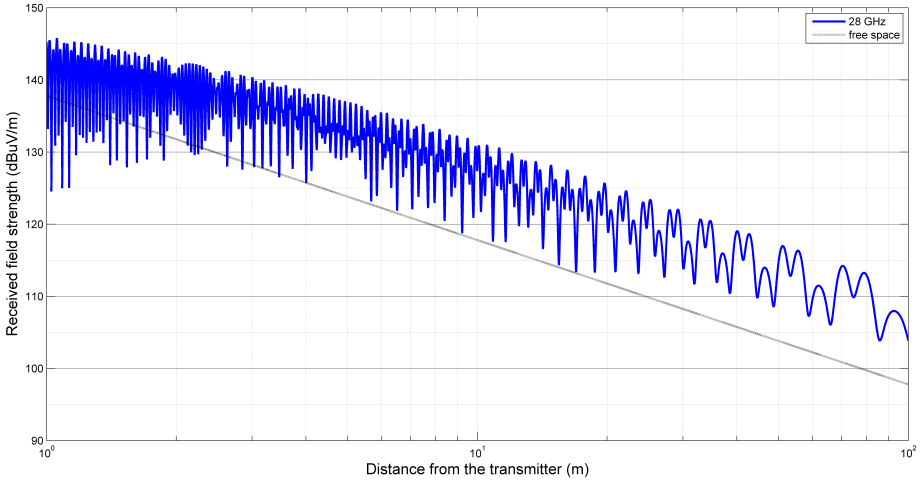

(c) 28 GHz

Figure 4.5: Path loss curves for physical model

There is much multipath in the corridor, as there is a large number of dips on the curves in the previous figures. Furthermore, the number is getting bigger with the increasing frequency. The model also shows that the power decay is slower than in the free space, due to waveguide effect.

4.4.2 Empirical model

For a demonstrative implementation of empirical models was selected One-Slope model stated in Section 4.3.1, which is characterized especially by the simplicity of calculation. Mean value of the path loss is given by Equation 4.6, the reference path loss L_1 at distance of 1 m is given by Equation 4.5. The value of the path loss coefficient for the case inside the building with a line of sight according to [1] is 1.6-1.8 and for the implementation was selected n = 1.7. The value of the path loss exponent, however, will be different for different frequency and therefore is considered to be calibrated according to the measured values. In this case, we will set distance range from 1 to 100 meters. The output of the model is a dependency of the path loss on the distance as it shows the Fig. 4.6. As we can see, the empirical model does not take into account multipath propagation, which causes the increases and dips of received power at certain distances in the physical model. The model gives the information only about overall power level and about the various decay for different frequencies.

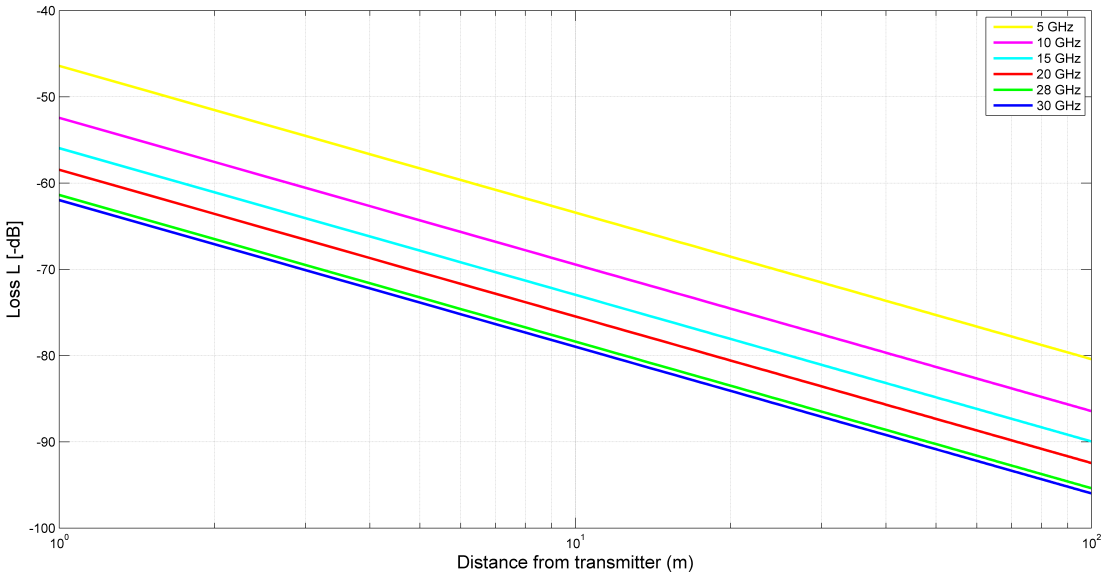

Figure 4.6: Empirical One-Slope model, n=1.7

Chapter 5

Measurements

5.1 Assumptions

The aim of this work is to find out how the radio signal is impacted not only by the distance it travels but also how it is influenced by the environment in which it travels. Of particular interest for next generation communication systems are frequencies up to 40 GHz. The measurements were conducted in two different environments - corridor and the office-like environment and was made to characterize both large- and small-scale propagation effects caused by the environment.

To characterize large-scale effects, the transmitter (TX) was fixed in the environment of interest. The receiver (RX) was moved to multiple distances (T-R distances) from the TX. Small-scale effects are characterized using three methods to account for spatial, temporal and frequency effects.

Measurements of the large-scale effects in the corridor were conducted separately, and it is the only measurement carried out using a spectrum analyzer. Due to its limitation, this measurement is carried out up to 30 GHz only. The other measurements were conducted more recently using vector network analyzer (VNA). The reason of utilization of the vector network analyzer is a lack of synchronization between spectrum analyzer and signal generator and wider frequency range of the VNA. The measurements using VNA were conducted in the whole frequency range from 5 GHz to 40 GHz, but only a few frequencies are presented in the thesis to maintain the brevity. The presented frequencies were chosen with respect to technologies operating on higher frequencies. The frequency 5 GHz is used in WiFi standard 802.11ac [6] as the next step after 802.11n, currently the most used standard. According to [7], the frequency of 10 GHz is allocated for fixed and mobile satellite services. And the 28 GHz band is a leading contender for 5G systems in Korea, US, and Japan [8]. Furthermore, wherever it is possible due to dynamic range, we picked the frequency of 40 GHz as another contender for the 5G system.

Each of the test scenarios has specific properties. Therefore, descriptions are given in the following text for each of them separately. All the measurements were conducted using Double Ridge Horn (DRH) antennas, which do not produce as much multipath as would be experienced using omnidirectional antennas. As the vast majority of mobile devices using some kind of omnidirectional antenna, it would be better conducting the measurement with such antennas.

The measurements were conducted on the premises of the Faculty of Electrical Engineering of CTU in Prague, Block B2, in the corridor on the 6th floor.

5.2 List of measurement instruments

- **Signal generator Keysight (Agilent) E8257D**
  Microwave analog signal generator with high output power, low phase noise, and modulation capability.
  Frequency range: 250 kHz – 50 GHz.
  Modulation AM, FM, PM.
  Interfaces - LAN and GPIB.
- **Spectrum analyzer Rohde&Schwarz FSP**
  Spectrum analyzer with frequency range 9 kHz – 30 GHz.
- **Vector network analyzer Rohde&Schwarz ZVA 40**
  Vector network analyzer with 2 test ports.
  Frequency range: 10 MHz to 40 GHz
- **Antennas DRH10 (Double Ridged Horn)**
  A pair of identical double-ridged horn antennas with a frequency range from 740 MHz to 10.5 GHz.
  Dimensions: width 204 mm, height 148 mm, depth 242 mm
- **Antennas DRH40 (Double Ridged Horn)**
  A pair of identical double-ridged horn antennas with a frequency range from 4 GHz to 40 GHz.
  Dimensions: width 52 mm, height 44 mm, depth 64 mm
- **Antennas DRH50 (Double Ridged Horn)**
  A pair of identical double-ridged horn antennas with a frequency range from 4.5 GHz to 50 GHz.
  Dimensions: width 52 mm, height 44 mm, depth 64 mm
- **Cables**
  Coaxial RF cables K (2.92 mm)

5.3 Long Corridor

5.3.1 Large scale effects

The measurement was divided into two frequency bands so that the available double ridged horn antennas (DRH 10 and DRH 40) can cover the given frequency range:

- frequency range 5 GHz to 10 GHz
- frequency range 10 GHz to 30 GHz

Chosen way of measurement is very simple. The measurement is based on sweeping the frequency of signal generator with step 1 GHz. The radio signal from the generator is applied to the antenna through coaxial RF cable, which radiates the energy as electromagnetic waves to the space of a corridor.
There is the same antenna connected to the spectrum analyzer on the receiving side. Simplified diagram and photo of the measurement system are shown in Figs. 5.1:

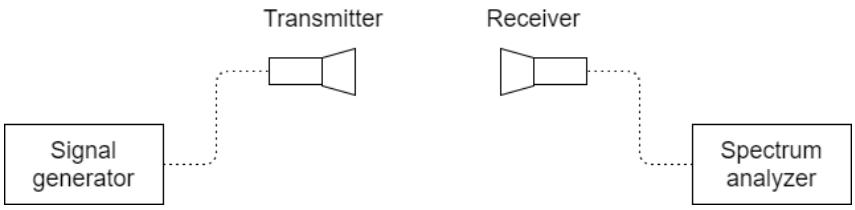

Figure 5.1: Simplified diagram of the measurement system

Spectrum analyzer records the frequency range in cycles and using the function MAX-HOLD displays the received signal level for the whole frequency band. After sweeping the whole range, data set is stored in a USB memory drive. The receiver is placed on the roadworthy table, that is traveling with the given step between the antennas. The position of the antennas in the corridor and the dimensions of the corridor are shown in Fig. 5.3. The measurement was carried out to a T-R distance of 28 m. During the measurement, we were changing the value of the attenuator, making sure that the measurement will take place continuously above the noise level. Photography of the measurement system placed in the corridor is in Fig. 5.2.

Figure 5.2: Measurement system

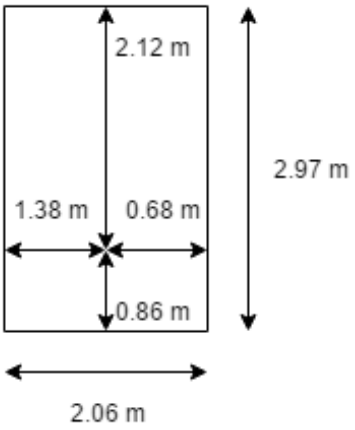

Figure 5.3: Position of the antennas in the corridor

The measurements were carried out for a total of 25 different frequencies; only a few selected frequencies will be illustrated by figures in the following text. The calculated values of the path loss exponent and other parameters necessary for the evaluation of the measurement and the comparison with implemented models will be listed for all the measured frequencies in the form of tables.

In sub-figures of Fig. 5.4, the measured values of received power dependent on the distance from the transmitting antenna for several different frequencies are presented. The measured data shows how the propagation is impacted by multipath. Dips and tops are present as the destructive interference applies in particular due to reflections from the wall. This phenomenon is more obvious at longer distance with increasing frequency. In Fig. 5.4a, the waveguide effect applies at approx 3.5 m at frequency of 5 GHz, while the same effect applies at 6 m at frequency of 28 GHz. Each sub-figure also contains the comparison to the empirical model with the path loss exponent independent on the frequency as it was presented in the section 4.4.1.

Path loss exponent is calculated as the slope of the line, which is a linear approximation to the measured values solved with a method of the least squares. As we can see in Table 5.1, path loss exponent is below than two, which is a valid value for free space. This fact is related to the expected wave propagation along the corridor, where the power decay is slower thanks to the waveguide effect. Apart from investigating ‘measured‘ path loss exponents, we can compare the measurement to empirical model using standard deviation σ. Standard deviation is given by the formula:

$$\sigma = \sqrt{\frac{1}{N-1}\sum_{i=1}^{N}(x_i - y_i)^2} \tag{5.1}$$

where N is a quantity of data set values, x_i is the values of data set, y_i is approximated function, in our case, the approximated function is our simulation output.

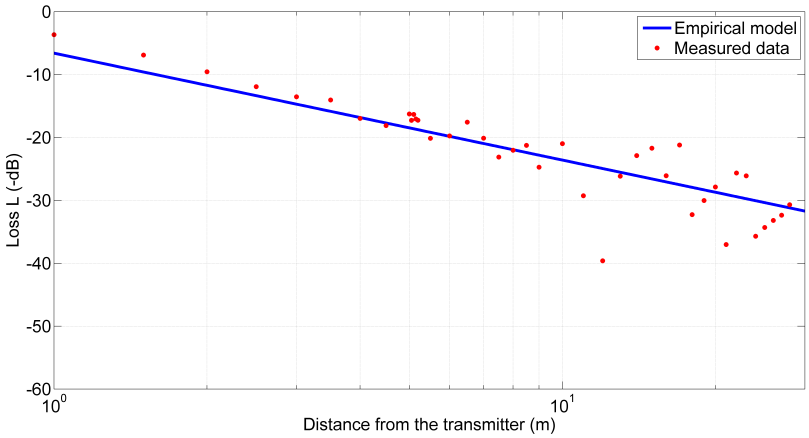

(a) Frequency 5 GHz, n=2.01, σ=3.8 dB

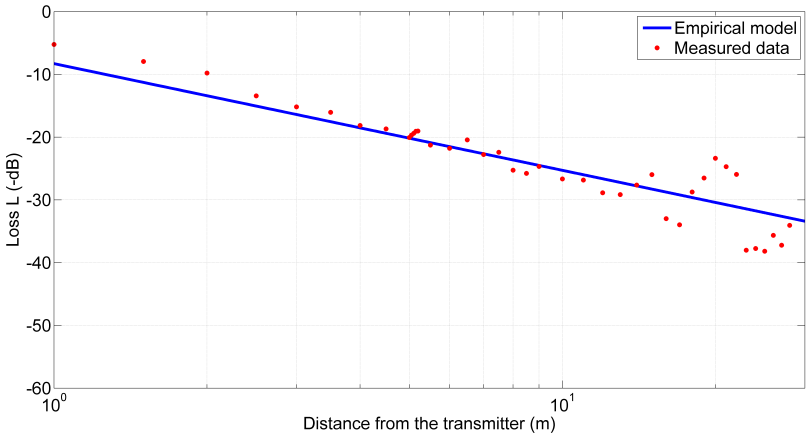

(b) Frequency 10 GHz, n=2.04, σ=3.2 dB

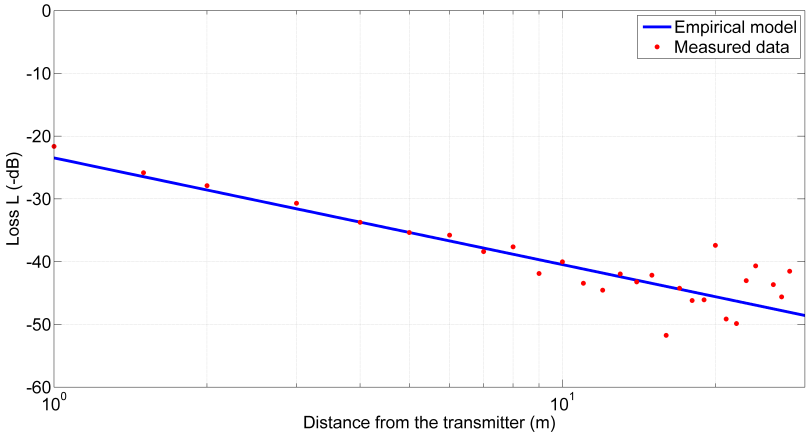

(c) Frequency 28 GHz, n=1.75, σ=4.2 dB

Figure 5.4: Comparison - measured data and empirical model

Frequency [GHz]	Path loss exponent n[-]	Standard deviation σ [-]
5	2.01	3.8
6	1.93	3.9
7	1.70	3.8
8	1.95	3.6
9	1.89	3.8
10	2.04	3.2
11	1.88	5.4
12	1.75	3.6
13	1.93	4.6
14	1.75	4.1
15	1.89	5.1
16	1.71	4.1
17	1.95	3.8
18	1.72	3.8
19	1.76	4.3
20	1.67	5.4
21	1.88	5.8
22	1.80	3.6
23	1.96	5.2
24	1.89	2.9
25	2.19	6.7
26	2.06	4.1
27	1.75	5.1
28	1.75	4.2
29	1.89	3.3
30	1.97	4.3

Table 5.1: Calculated values of path loss exponent obtained from the measured data

It is common to make a calibration of the empirical model using parameters obtained during the experimental measurement. In our case, we make calibration using 'measured' path loss exponent instead of frequency independent one. When we make this calibration, we get new values of standard deviation. In Table 5.2, the values of standard deviation differs only by a couple of tenths of a decibel. As the empirical model does not take into account the reflections and other mechanisms of the propagation, the value of n does not influence the values of standard deviation. Therefore, the calibration is not useful in our case, so there are no figures with a comparison of the measured data to calibrated empirical model, which would be pretty the same as the comparison to the original empirical model. Table 5.2 also summarizes whole comparison, values of path loss exponent for calibrated empirical model are same as the values obtained from the measurement. Therefore there is no separate column for "measured" path loss exponent.

When comparing the physical model to the measurement data, we compare only path loss exponents. The graphical comparison is shown in Figs. 5.5a, 5.5b, 5.5c. Calculated path loss exponent for the physical model is shown in final Table 5.2.

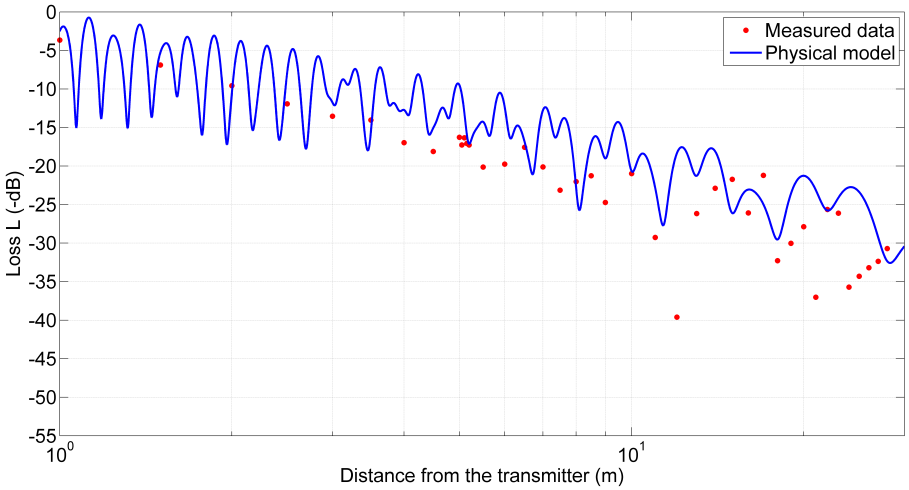

(a) Frequency 5 GHz

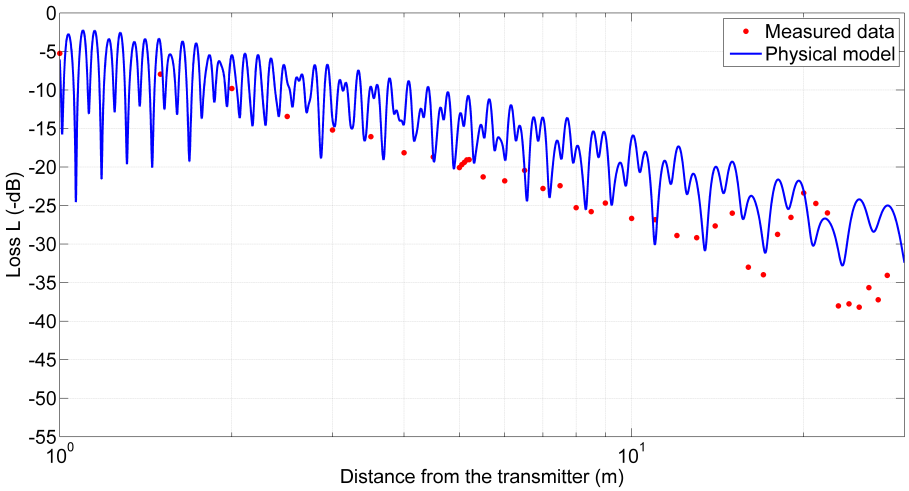

(b) Frequency 10 GHz

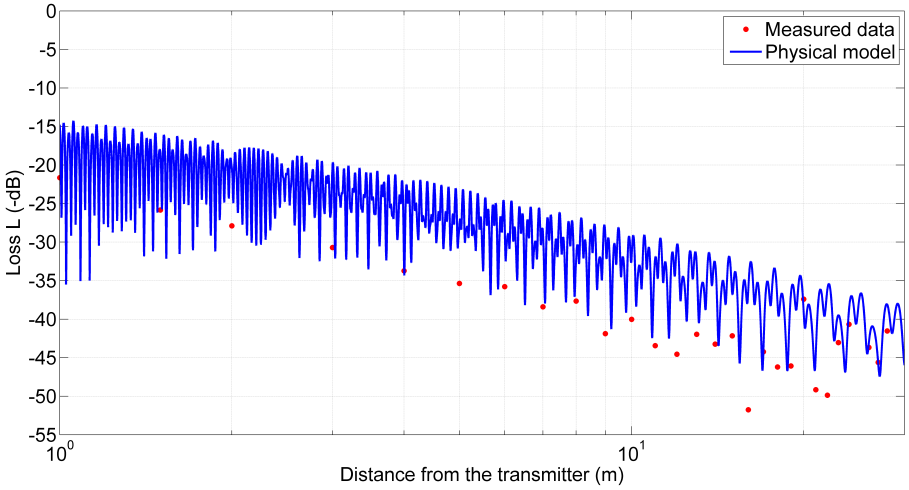

(c) Frequency 28 GHz

Figure 5.5: Comparison - measured data and physical model

	Empirical model from literature		Calibrated empirical model		Physical model
f [GHz]	n [-]	σ [dB]	n [-]	σ [dB]	n [-]
5	1.70	3.8	2.01	3.6	1.78
6	1.70	3.9	1.93	3.8	1.65
7	1.70	3.8	1.70	3.8	1.80
8	1.70	3.6	1.95	3.5	1.82
9	1.70	3.8	1.89	3.7	1.69
10	1.70	3.2	2.04	2.9	1.72
11	1.70	5.4	1.88	5.3	1.83
12	1.70	3.6	1.75	3.6	1.79
13	1.70	4.6	1.93	4.5	1.75
14	1.70	4.1	1.75	4.1	1.80
15	1.70	5.1	1.89	5.4	1.63
16	1.70	4.1	1.71	4.1	1.76
17	1.70	3.8	1.95	3.7	1.82
18	1.70	3.8	1.72	3.8	1.78
19	1.70	4.3	1.76	4.3	1.75
20	1.70	5.4	1.67	5.4	1.85
21	1.70	5.8	1.88	5.0	1.73
22	1.70	3.6	1.80	3.6	1.77
23	1.70	5.2	1.96	5.1	1.83
24	1.70	2.9	1.89	2.8	1.70
25	1.70	6.7	2.19	6.4	1.78
26	1.70	4.1	2.06	3.9	1.77
27	1.70	5.1	1.75	5.1	1.77
28	1.70	4.2	1.75	4.2	1.83
29	1.70	3.3	1.89	3.2	1.75
30	1.70	4.3	1.97	4.2	1.72

Table 5.2: Final summary

The measurement was carried out with rather sparse distance step as the measurement system was very simple and provisional. The step should be much more dense to precisely measure the large effects, especially in such high-frequency bands.

5.3.2 Small scale effects

Measurement principle

From this measurement onwards, the measurement was conducted using the VNA, because of inadequate dynamic range of the spectrum analyzer, the absence of the synchronization between the spectrum analyzer and signal generator, and to measure at higher frequencies (up to 40 GHz). The principle of the measurement was pretty similar to the measurement with the spectrum analyzer. The measurement is based on sweeping the frequency of the output signal of the VNA; the signal is applied to the TX antenna (DRH 50) connected to the Port 1, which radiates the energy to space towards the RX antenna of the same type connected to the Port 2. The VNA measures parameter S_{21}. The simplified diagram is shown in Fig. 5.6 and the photography in Fig. 5.7.

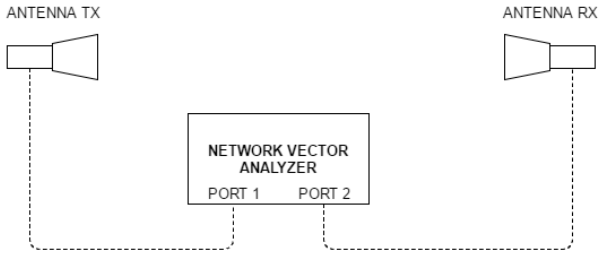

Figure 5.6: Diagram of the measurement system

Figure 5.7: Photography of the measurement system

The VNA settings:

- Power: 15 dBm
- RBW: 100 Hz
- Frequency step: 10 MHz
- Frequency range: 5 to 40 GHz
- Sweep: 3501 points

We use three measurement methods to characterize the small-scale effects to account spatial, temporal and frequency effects. Measured data are compared to well-known Rayleigh fading model using cumulative distribution functions (CDF). Each data set is normalized by the median, so all curves pass through the crossover point (0 dB - median, 50% probability).

Spatial effects

The receiver is moved short distances without changing the T-R distance to account spatial variability as shown in Fig 5.8a, the antennas do not point at each other, except the initial position, when both antennas were in the middle of the corridor. As we can see, we move RX antenna along the straight line because we measure in the antenna's far field and electromagnetic waves can be considered as the plane waves. Both antennas are placed on tripods, the position of RX is changed from one corridor wall to the other wall with 2 cm step. There was a total of 77 points measured within the measurement. The fixed T-R distance is stated as 7 m, and the antennas are at the height of 1.34 m as shown in Fig. 5.8b.

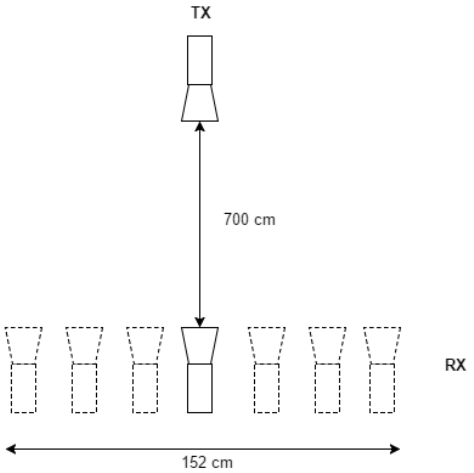

(a) Top view

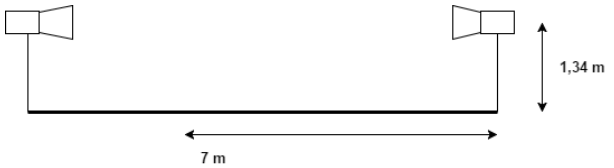

(b) Side view

Figure 5.8: Spatial effects

Measured spatial effects are displayed in Fig. 5.9 where we can see deeper fades near the walls than in the middle of the corridor. When we compare our and Rayleigh scenarios, as shown in Fig. 5.10, the fading is less severe with the higher frequency, because there is a greater counterclockwise rotation of the CDF curve about the crossover point. It means the higher the frequency, the lower fade margin is needed. For example, to achieve the outage probability of less than 3%, a system operating at 5 GHz needs to have approx. 17 dB fade margin (relative to median value 0 dB). While the system operating on the 40 GHz needs only 7 dB fade margin needs to be considered during the system design. For the scenario of the system operating on 5 GHz, there is more severe fading than for the Rayleigh scenario, where for example the probability of less than 2%, for our system needs to be considered 7 dB higher fade margin than in the Rayleigh environment. This is an example of the hyper-Rayleigh fading [4].The fading is shown in Fig. 5.9a, where we can see deep fades at several positions of the receiver (one of them is at distance of 160 cm).

Interesting behavior has the system operating on 28 GHz, the fading statistics are more severe than the predicted by the Rayleigh model for probability less than approx. 4%, while less severe for higher probability. It corresponds with the Fig. 5.9c, where there are only a few deep fades.

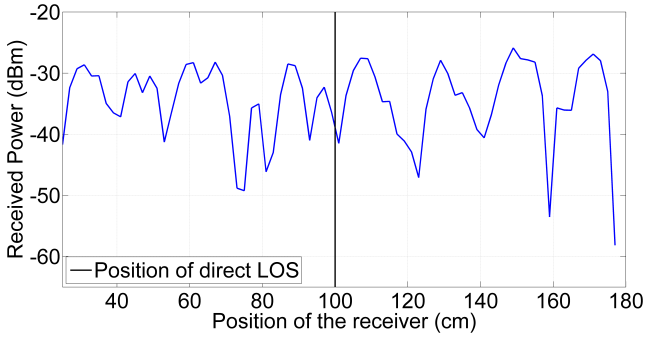

(a) 5 GHz

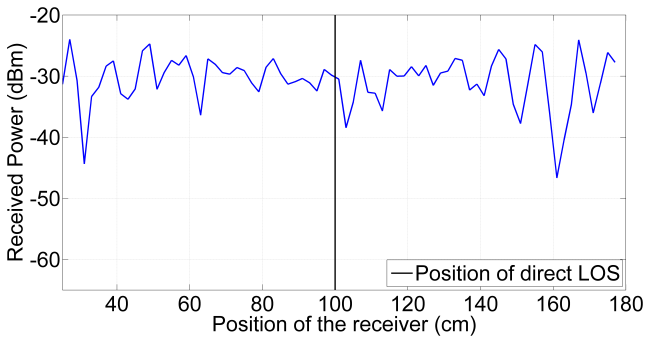

(b) 10 GHz

Figure 5.9: Spatial effects in the corridor

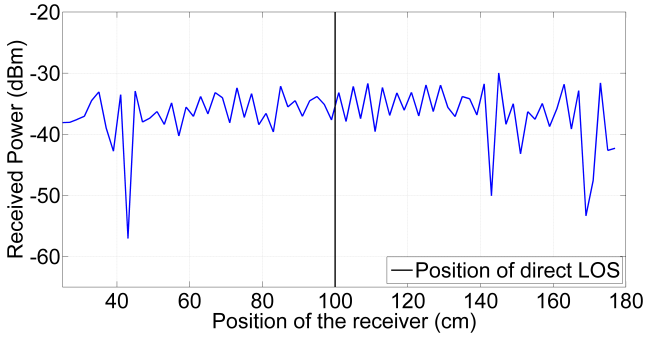

(c) 28 GHz

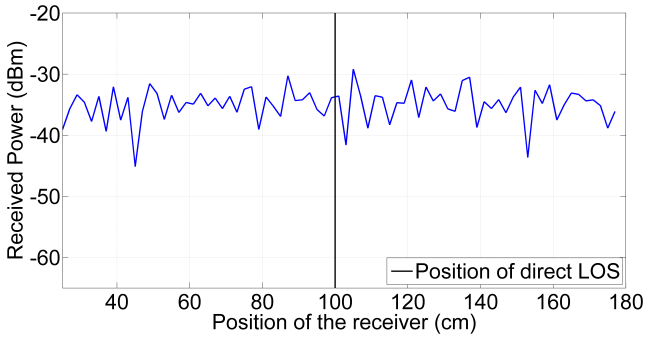

(d) 40 GHz

Figure 5.9: Spatial effects in the corridor (cont.)

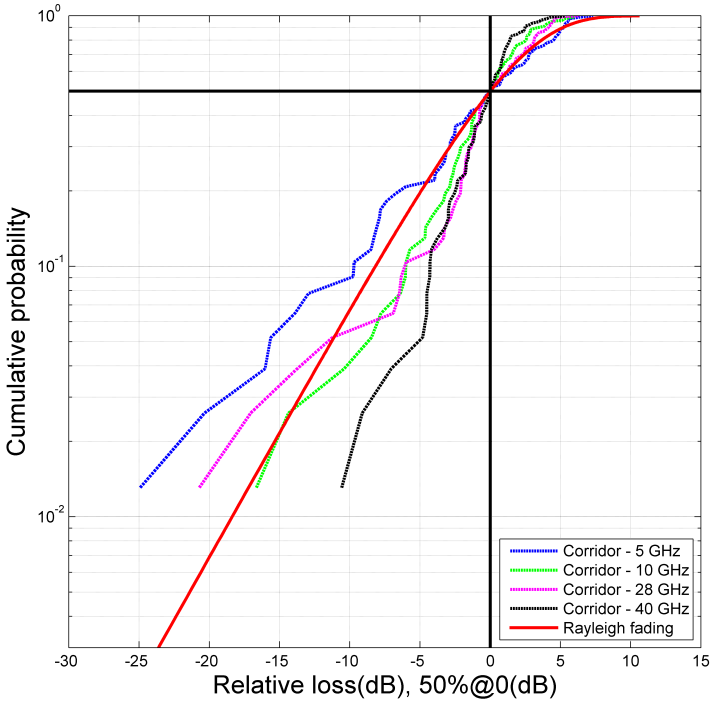

Figure 5.10: Spatial effects - Fading envelopes

Temporal effects

The setup of the devices is same as in the previous measurement. The RX antenna is placed in the middle of the corridor, and its position is fixed. The VNA is set on the single frequency, with the function MAXHOLD turned off. The time of the single measurement is set for 120 seconds, during this time the environment is changing through the motion of several volunteer walking between the antennas.

The measurement of the temporal effects is carried out on three frequencies - 5, 10, 28 GHz. The measurement at frequency 40 GHz is not carried out because at this distance and this frequency there is a lack of dynamics of the VNA, where some of the deepest fades were below the noise level. In 5.11, the comparison across the frequency is not really fair, as each frequency is seeing a different 'movement pattern.' On the other hand, we can compare fading envelopes. In Fig. 5.12, all fading envelopes are very similar to the envelope of the Rayleigh environment, and all the scenarios have less severe fading in general. It means that temporal effects on the corridor are same at these frequencies and there will be no difference of the necessary fade margin of the system in a corridor on different frequencies. The Rayleigh fading is the typical condition assumed for mobile channels. Thus the measured temporal effects show, movement in the corridor environment does not create more severe fading than assumed Rayleigh.

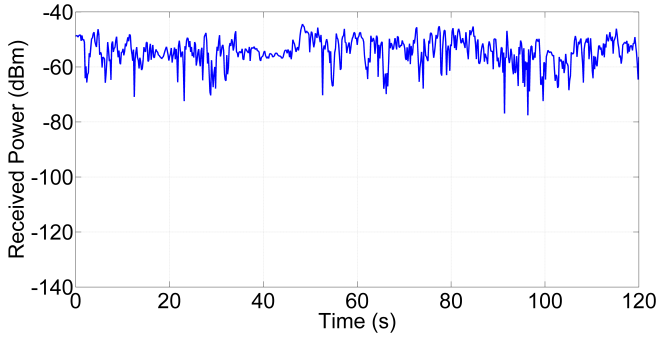

(a) 5 GHz

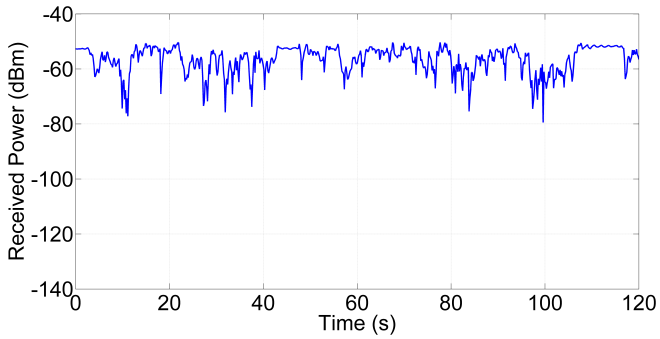

(b) 10 GHz

(c) Temporal effects in the corridor

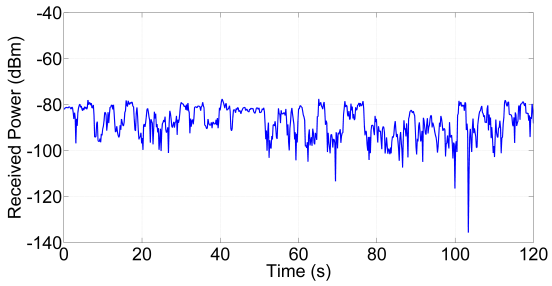

(d) 28 GHz

Figure 5.11: Temporal effects in the corridor (cont.)

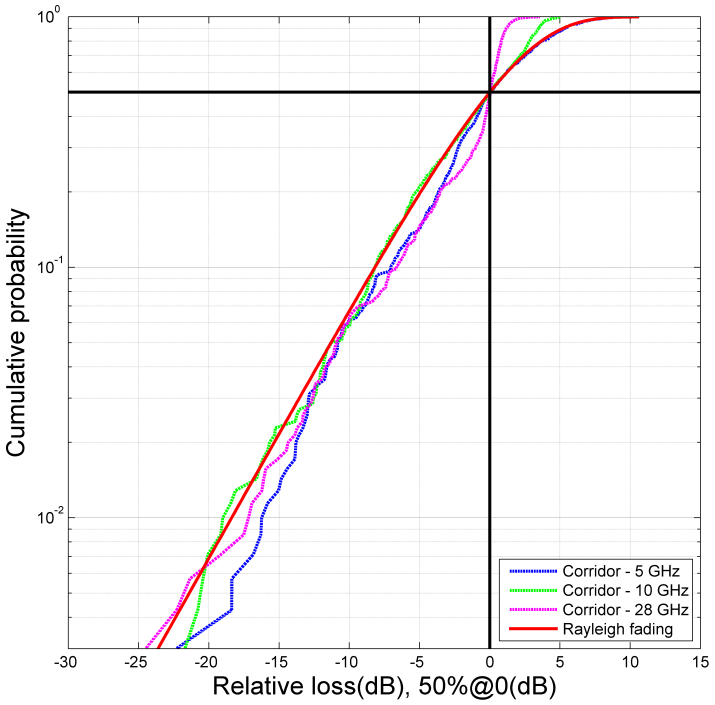

Figure 5.12: Temporal effects - Fading envelopes

Frequency effects

A sweep over the whole frequency range 5 to 40 GHz was conducted in this part. In Fig. 5.13 we can clearly see the dips (fades) at certain frequencies due to the reflections in the corridor. These reflections are causing destructive interference, so we can observe those dips we mentioned before. We can see that the overall level of the received power is descending as well.

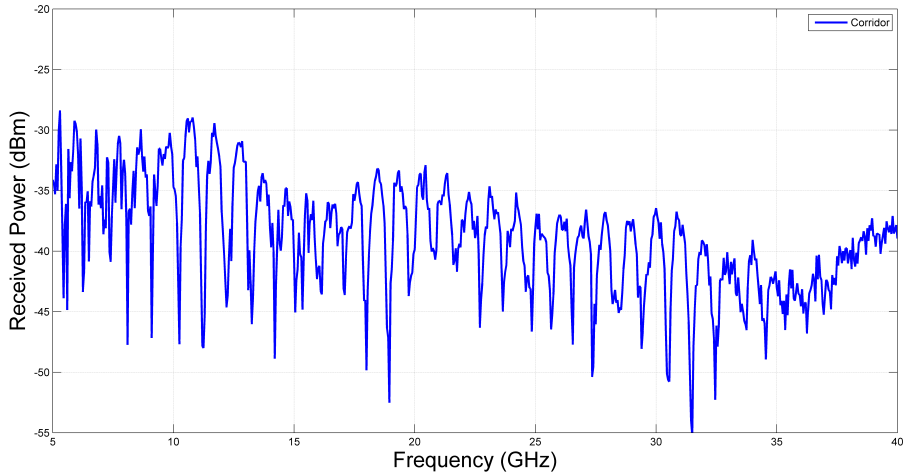

Figure 5.13: Frequency effects

In Fig. 5.14, the fading looks like the Ricean fading with low Ricean factor $K_r \approx 1dB$. The factor was calculated using the 10% fade depth metric [9]. The factor equals the ratio of the power in the LOS component to the power in the diffuse component [1]:

$$K_r = \frac{A^2}{2\sigma^2} \tag{5.2}$$

where A means the amplitude of the dominant component and σ^2 denotes the variance.

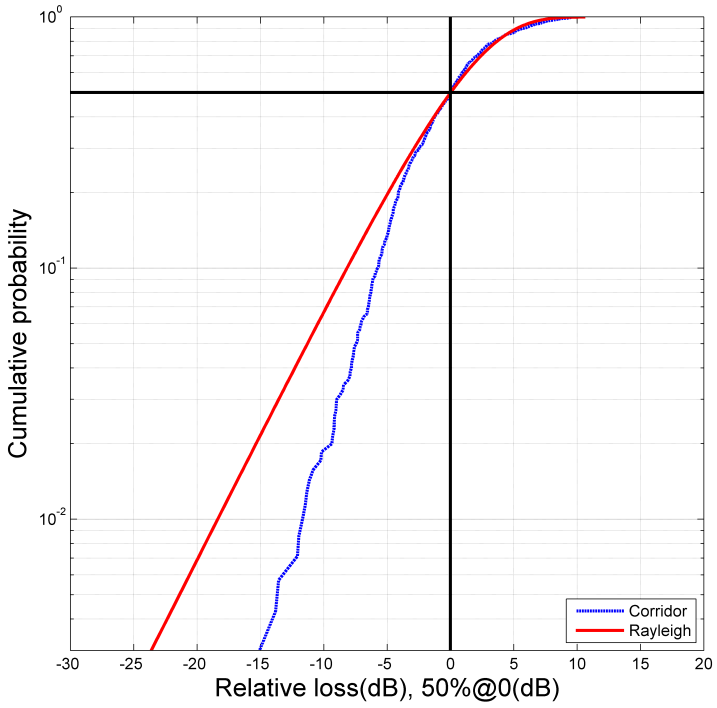

Figure 5.14: Frequency effects - Fading envelope

5.4 Office-like environment

The principle of each measurement is the same as in the case of the corridor, yet the environment is changed. The measurement was conducted in an environment similar to the ordinary office environment, which contains a lot of furniture, windows and other various objects, as in Fig. 5.15. Many reflections, refraction, diffractions can occur in such an environment.

Figure 5.15: Measurement system

5.4.1 Large scale effects

We change the T-R distance with the step of 10 cm, starting distance is 1 m, as the criterion of the far field of the antenna is met, and final distance is 5 m. The measured frequency band is 5 GHz to 40 GHz. As in the case of the corridor, the path loss exponent is calculated, this time only for a few frequencies from range 5 GHz to 40 GHz as obviously the exponent does not change much in this environment. The values of the path loss exponent presented in Table 5.3 are very close to the value of the exponent for free space n=2 and are slightly below this value for higher frequencies. In comparison to the corridor, there is no significant multipath propagation in the environment of the office. In Fig. 5.16, only wanted frequency data sets are presented. There are not many dips on the curves because there almost is no influence of the reflections, so the destructive interference of the waves cannot succeed, all this due to the type of used antennas

In general, we can say the multipath is not present in the office-like environment because we used the antenna with pretty narrow beams.With such antennas, we cannot achieve such reflections from the walls as we could with omnidirectional antennas, typical for wireless communication devices.

f [GHz]	Path loss exponent [-]
5	2.05
10	2.02
15	1.98
20	1.96
25	2.02
28	1.96
35	1.97
40	1.97

Table 5.3: Path loss exponent values

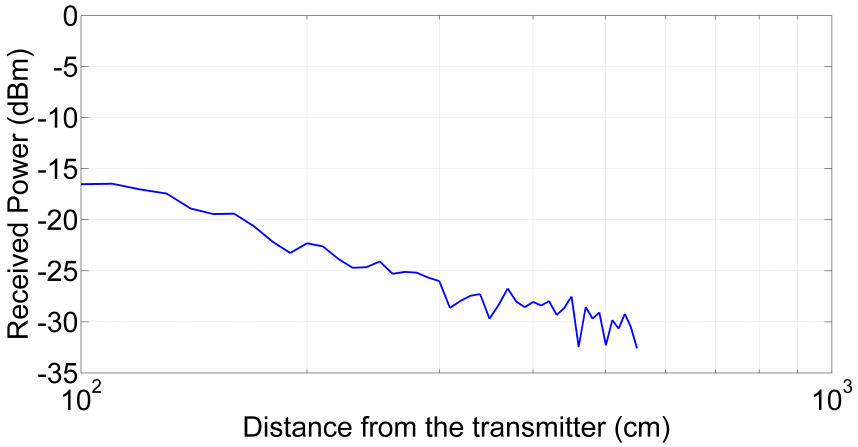

(a) 5 GHz

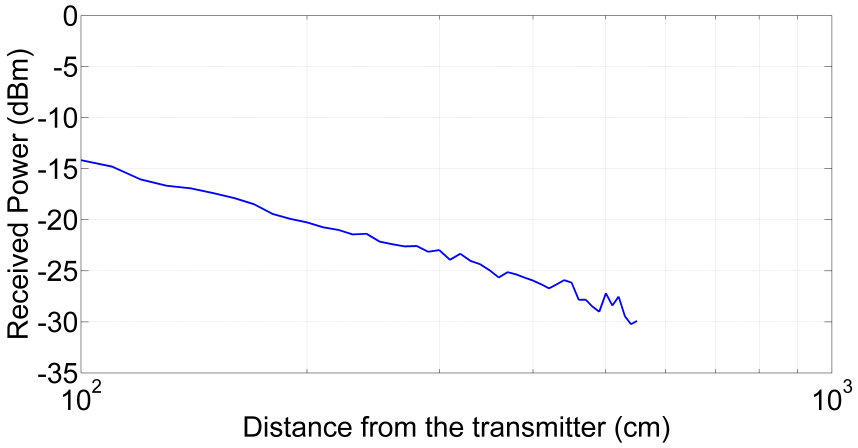

(b) 10 GHz

Figure 5.16: Large scale effects in the office

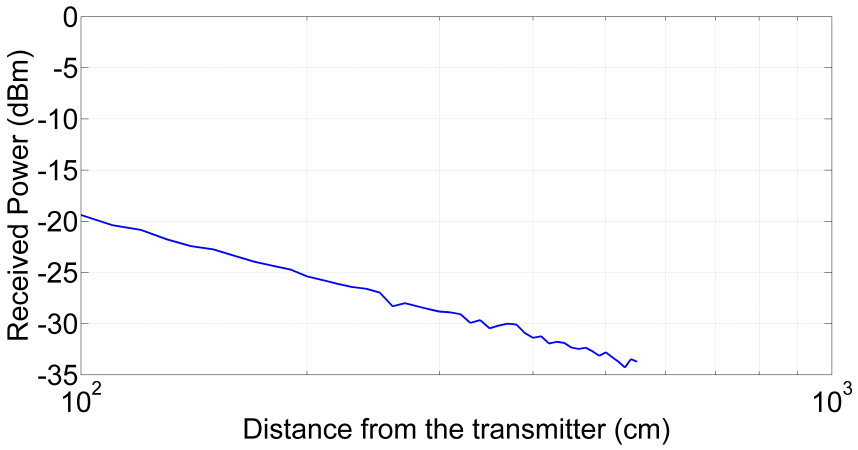

(c) 28 GHz

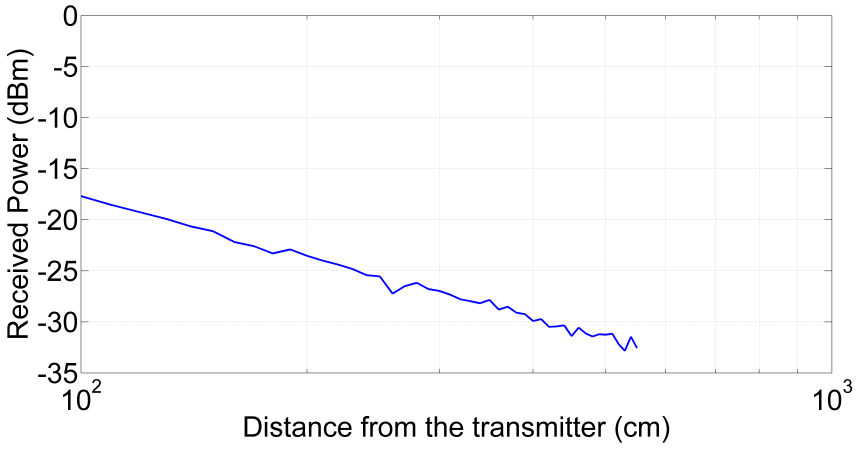

(d) 40 GHz

Figure 5.16: Large scale effects in the office (cont.)

5.4.2 Small scale effects

Spatial effects

As the environment has changed, the spatial range has changed as well, as shown in Fig. 5.17. There is no difference between the measurements in the corridor and in the office except the changed spatial range.

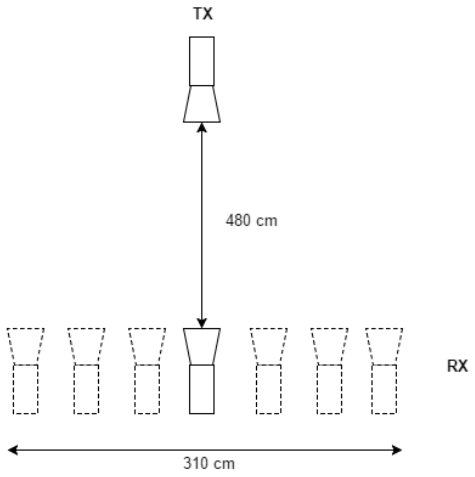

Figure 5.17: Measurement of the spatial effects

In Fig. 5.18, there is the obvious influence of the beam width of the available antennas, as the level of the received power drops with the distance from the direct LOS. This phenomenon is more apparent with the increasing frequency, as in Fig. 5.18d, where the drop of the signal level for frequency 40 GHz is not caused only by the spatial effects, but it is mostly linked with the beam width of the antennas only. Therefore, in Fig. 5.19, the CDF curve for 40 GHz cannot be interpreted as the more severe fading than the Rayleigh fading. Assume the beams for three remaining frequencies are wide enough, so the fading statistics are influenced only by the spatial effects. As we see, the fading statistics of this scenario is much less severe than the statistics of the Rayleigh channel. For example, the difference between fade margins of the 5 GHz system and Rayleigh system for the outage probability less than 2% is approx 12 dB. The system operating at the frequency of 5 GHz as well as the systems at 10 GHz and 28 GHz, are similar to Ricean fading model, with high Ricean factor $K_r \approx 6$dB [9]. It means the dominant multipath component is present, in our case it would be the component of the direct LOS.

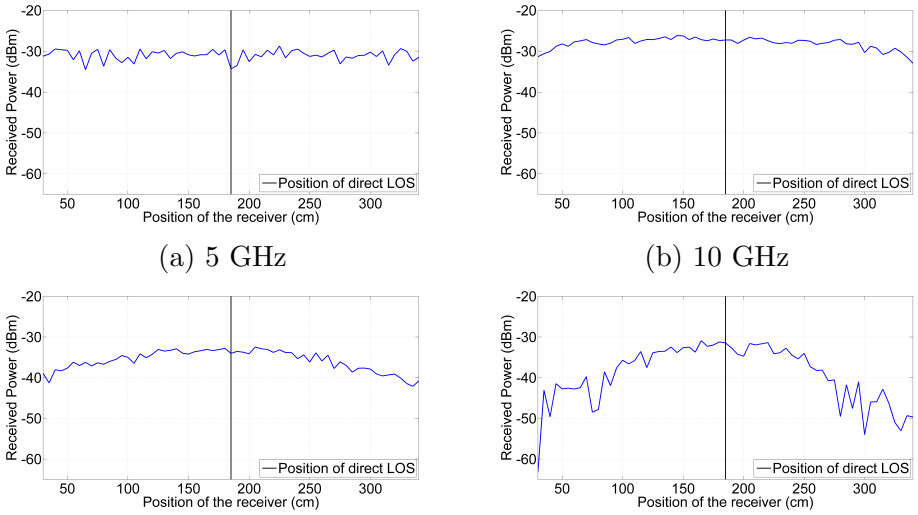

(a) 5 GHz (b) 10 GHz

(c) 28 GHz (d) 40 GHz

Figure 5.18: Spatial effects in the office

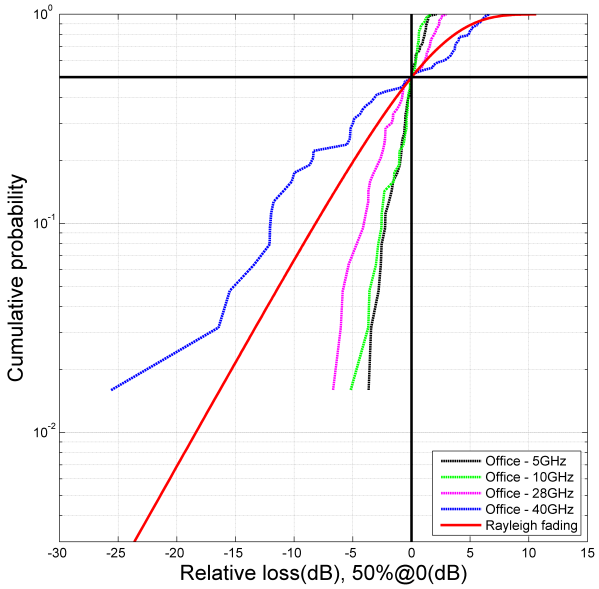

Figure 5.19: Spatial effects - Fading envelopes

The omnidirectional antenna would be much more better to measure spatial effects in the office as for almost every other measurement conducted as a part of this thesis.

Temporal effects

Measurement of the temporal effects in the office is completely the same measurement as in the corridor. There is a movement between the two antennas with fixed RX-TX distance for 120 seconds. In Fig. 5.20c, the intentional no movement in the direct LOS during the first 30 s of the measurement is presented. There are no fades at all during this time, as we can see, the signal level is constant in those times when there is no movement in the direct LOS for all frequencies. In Fig. 5.21, the no-movement situation is illustrated as almost the unit step up to a 70% of the time for the frequency of 28 GHz. It means there is just very little or no multipath, and direct LOS is dominant. The fading statistics are more severe at higher frequencies due to shadowing of the LOS and absence of the multipath.

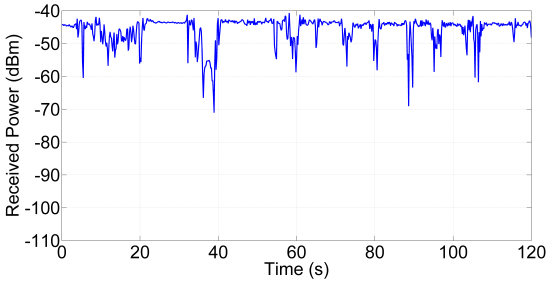

(a) 5 GHz

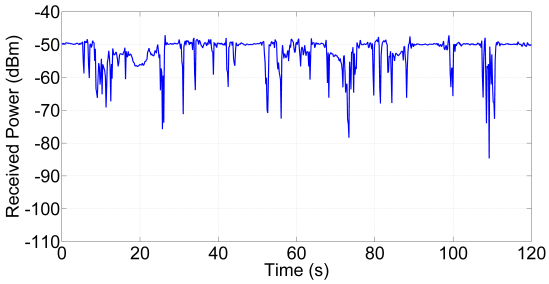

(b) 10 GHz

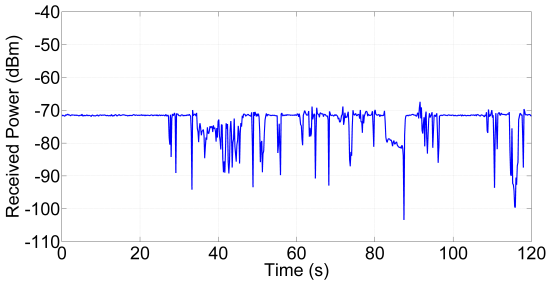

(c) 28 GHz

Figure 5.20: Temporal effects in the office

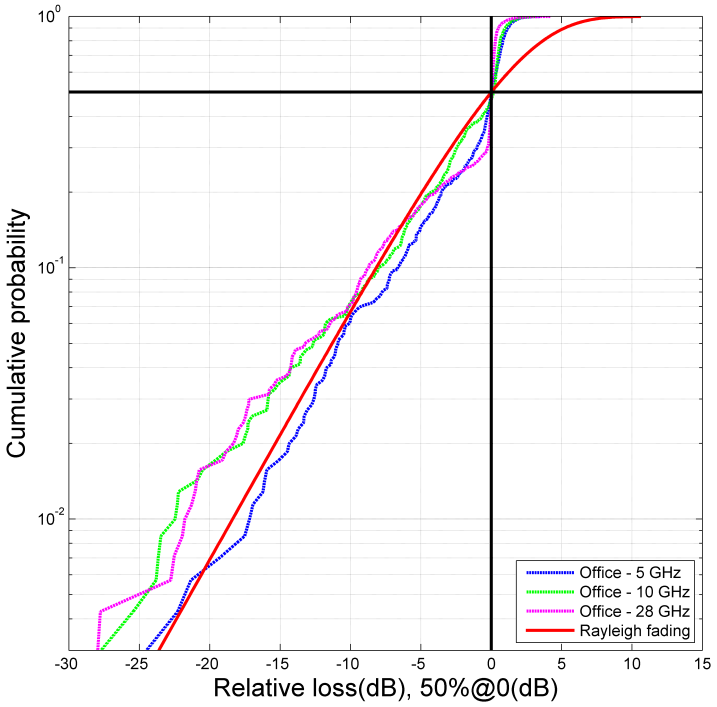

Figure 5.21: Temporal effects - Fading envelopes

Frequency effects

To characterize the frequency effects in the office we are turning the antenna off the LOS axis by ±15°, ±30°, ±45°, as shown in Fig. 5.22. We did this to introduce multipath propagation. Antennas in the position of direct LOS would not introduce the multipath due to their type. So, with the increasing angle off axis, more multipath propagation is expected as the electromagnetic wave incidents onto obstacle and reflection occurs.

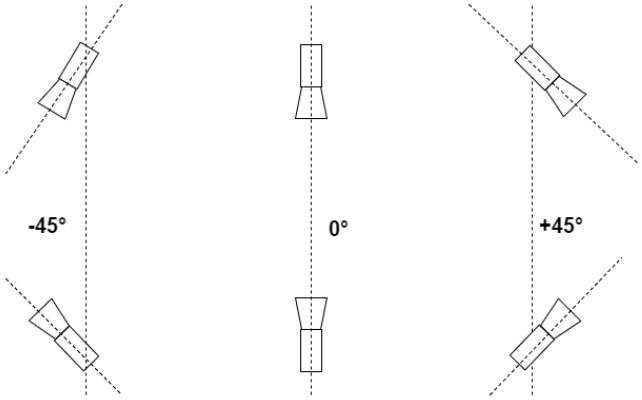

Figure 5.22: Measurement of the frequency effects

In Fig. 5.23, we do sweep over the frequency band 5 GHz to 40 GHz as in the corridor measurement. We can observe multipath propagation as the antennas are turned by 30° and 45°, while it is very little or none multipath when the antennas are just slightly turned. When we compare ‘plus‘ and ‘minus‘ turns, there is the obvious difference as the environment is different on each side of the office. There is a window on one side of the office when we turn the antenna by plus degrees, and there is a shelf with the various stuff when we turn the antenna otherwise. We can say that there is more complex multipath propagation on the side with the shelf, as the reflective area is much more ragged than the reflective area of the window. In general, the dips caused by destructive interference at certain frequencies, are more dense with the higher frequency.

When comparing fading envelopes, we break the records over three bands here (5 GHz to 10 GHz, 10 GHz to 20 GHz and 20 GHz to 40 GHz), as we can discuss different behavior as a function of frequency. In Fig. 5.24a, the antennas are in the direct LOS and almost no fading is present. When we turn both antennas by plus or minus 15° (Figs. 5.24b, 5.24c) the fading starts to get more severe as some multipath is present. With antennas turned by ± 30°, the fading envelopes are very similar to Rayleigh fading envelope. In this case, the multipath propagation is introduced, as it can be seen in Figs. 5.23b and 5.23c. Almost the same situation happens for angle 45°, with one difference. In Fig. 5.24g, one fading envelope is different from the others. The fading for frequency band 20 GHz to 40 GHz, is less severe than for the other bands. As it was mentioned before, ‘plus‘ turn means that the antennas are turning towards the window on one side of the office. As the antennas are initially placed parallel with the window, the turn by +45 degrees could mean, that only one reflection occurs in this situation.

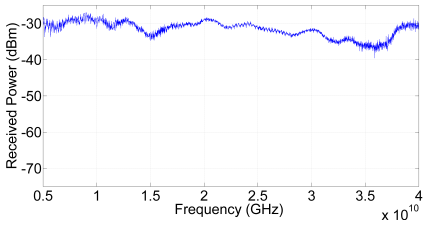

(a) Antennas turned by 0°

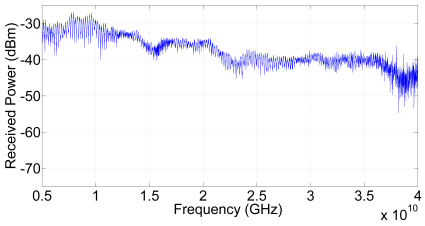

(b) Antennas turned by -15°

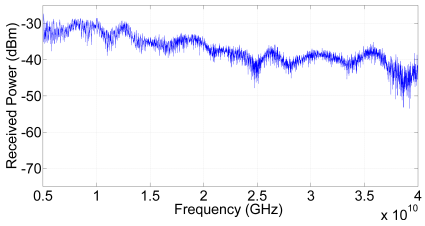

(c) Antennas turned by +15°

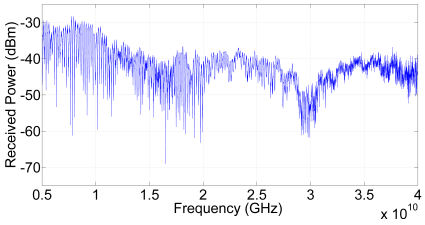

(d) Antennas turned by -30°

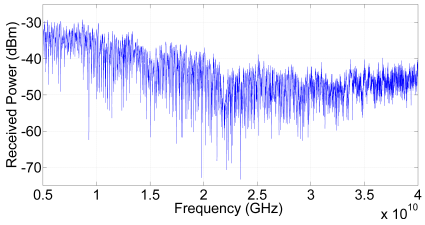

(e) Antennas turned by +30°

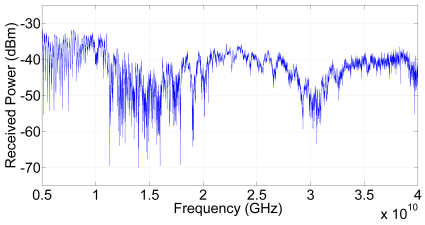

(f) Antennas turned by -45°

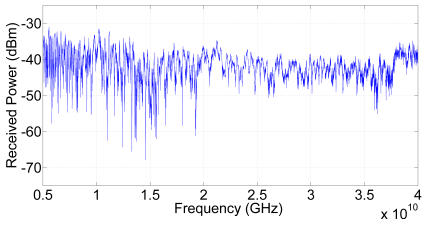

(g) Antennas turned by +45°

Figure 5.23: Frequency effects in the office

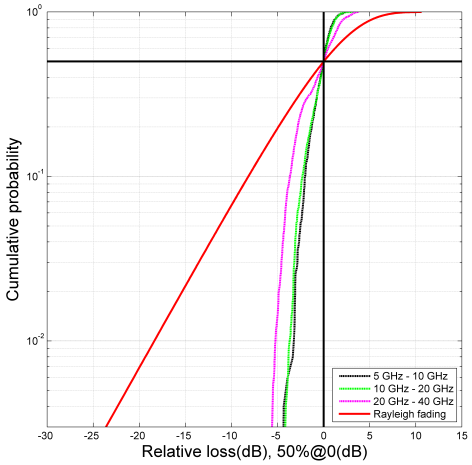

(a) Antennas turned by 0°

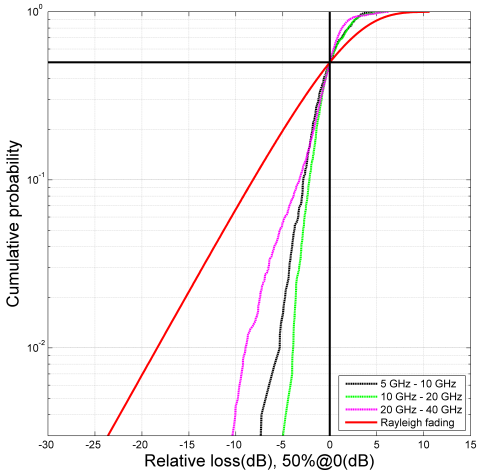

(b) Antennas turned by -15°

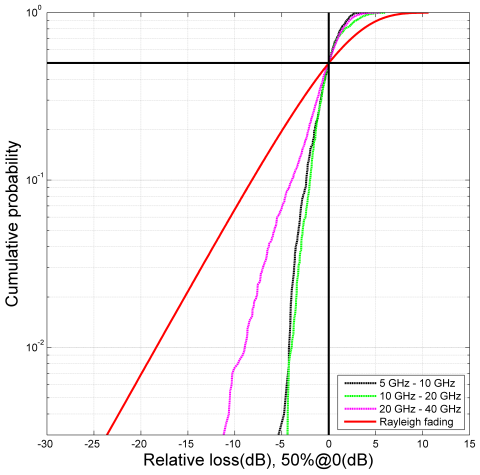

(c) Antennas turned by +15°

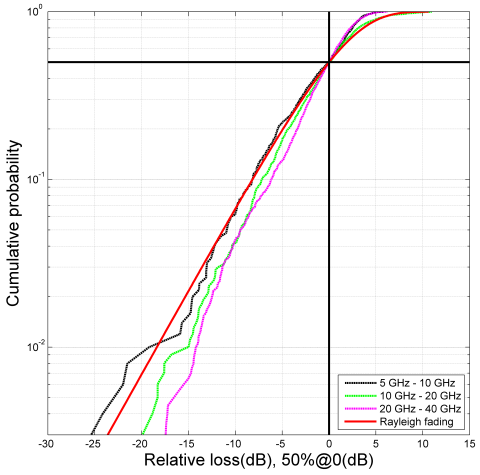

(d) Antennas turned by -30°

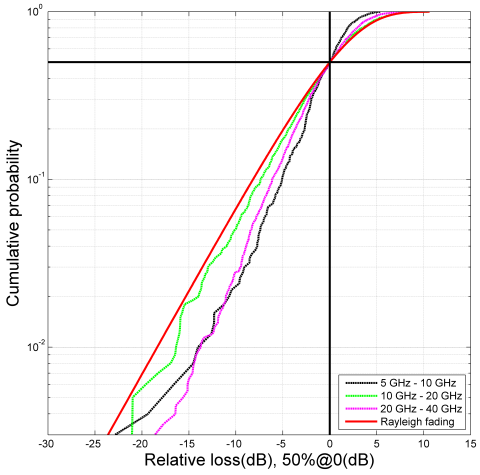

(e) Antennas turned by +30°

Figure 5.24: Frequency effects - fading envelopes

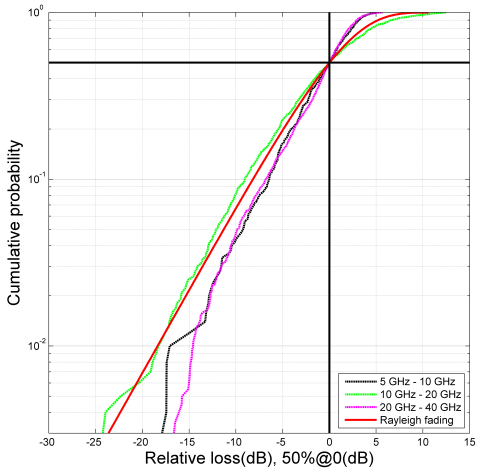

(f) Antennas turned by -45°

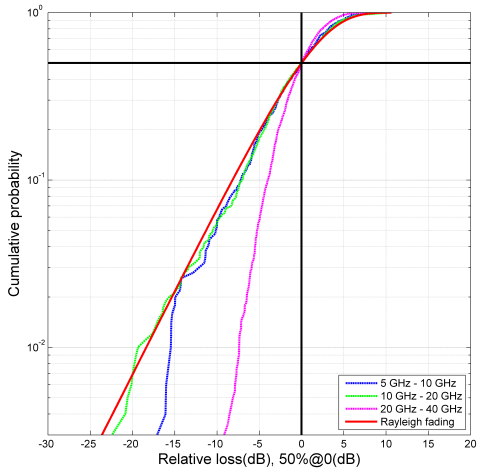

(g) Antennas turned by +45°

Figure 5.24: Frequency effects - fading envelopes (cont.)

5.5 Summary of the measurement results

The first way of the measurement was the measurement of the large scale effects in the corridor using the spectrum analyzer, where we wanted to verify this way of the measurement. The measured data indicated a presence of the waveguide effect for the first time in our measurements. The dips of the received power occurred significantly especially at higher frequency bands, as the multipath propagation was present. Moreover, the measurement data, presented in the section 5.3.1, substantially corresponds with the implemented propagation models and calculated path loss exponent also corresponds with the assumption of the waveguiding effect of the corridor.

The measurement conducted with vector network analyzer served to measure both the large and small scale effects in two environments - the corridor and the office-like environment. The large scale effects in the corridor were presented before. We measured the same effects in the office, and calculated path loss exponent was pretty similar to exponent for free space.

To determine small scale effects the measurement was split into three parts, to account spatial, temporal and frequency effects. Measured spatial effect shows, there is much more multipath propagation in the corridor than in the office, as the fading statistics of the office determine the dominant MPC like in the Ricean channel. There is no dominant MPC in the corridor like in the Rayleigh channel. There is little multipath propagation in the office, because of the type of used antennas and shorter range in which we conducted the measurement.

Temporal effects are pretty the same in both environments. Both measured effects are similar to Rayleigh scenario as expected. Nevertheless, it depends on where we move in the office-like environment. The movement outside of the direct LOS does not influence the signal level at all, as the multipath is not present once again. Frequency effects in the corridor show how the certain frequencies suffer from the destructive interference in the whole frequency range as the result of the multipath propagation. There is a different behavior in the office, as the effects depend on frequency and direct LOS differs from the off-axis angles of the antennas. These off-axis angles introduce the multipath propagation even with our narrow beam antennas.

The measurement can be considered as successful; the omnidirectional antennas can be used to better observe the effects, especially in the office-like environment.

Chapter 6

Conclusions

The main goal of the thesis was to summarize the behavior of the radio signal indoors and realize the measurement in high-frequency bands up to 40 GHz. The first part of the work, the theoretical introduction, contains the summary of the mechanisms occurring in radio channel inside the buildings. There is the statistical description of these mechanisms as well. Furthermore, the propagation models to predict some of the mechanisms, are presented in this part of the work.

As part of the work, two propagation models was implemented. These models are used to calculate the path loss exponents and further for comparison with measured large scale effects in the corridor. The measurement was split into several partial measurements to record different received power variations on both large and small scale. Two measurement procedures were proposed using a spectrum analyzer and vector network analyzer. As a gradual development, the method of measuring with the vector network analyzer was said as the best. As the available antennas were not omnidirectional, there is room for improvement of our measurement so it would be more realistic, as the vast majority of wireless devices use omnidirectional antennas.

In the end, it can be said that the thesis assignment was fulfilled both in theoretical and practical terms, where the measurement results can be considered as relevant.

Bibliography

[1] A. F. MOLISCH, *Wireless communications*. Wiley-IEEE Press, 2005, ISBN: 047084888X.

[2] P. PECHAČ and S. ZVÁNOVEC, *Základy šíření vln pro plánování pozemních rádiových spojů*. Praha: BEN - technická literatura, 2007, ISBN: 978-80-7300-223-7.

[3] S. R. SAUNDERS, *Antennas and propagation for wireless communication systems*, 1st. New York: John Wiley & Sons, Inc., 1999.

[4] J. FROLIK, "A case for considering hyper-rayleigh fading channels", *IEEE Transactions on Wireless Communications*, vol. 6, no. 4, pp. 1235–1239, 2007.

[5] P. PECHAČ, *Modely šíření vln v zástavbě: [modely pro plánování mobilních rádiových systémů : Wlan, wifi, dect, gsm, umts]*. Praha: BEN-technická literatura, 2005, ISBN: 80-7300-186-1.

[6] D. NGO, *5G Wi-Fi (802.11ac) explained: It's cool*, `https://www.cnet.com/news/5g-wi-fi-802-11ac-explained-its-cool//`, [Online; accessed 2017], 2012.

[7] F. C. Commission *et al.*, "Fcc online table of frequency allocations", *Online:[http://www.fcc. gov/oet/spectrum/table/fcctable. pdf]*, 2008.

[8] S. MAZUMDER, *5G New Radio – Emerging Spectrum Bands*, `http://blog.cartesian.com/5g-new-radio-emerging-spectrum-bands/`, [Online; accessed 2017], 2017.

[9] J. FROLIK, "A practical metric for fading environments", *IEEE Wireless Communications Letters*, vol. 2, no. 2, pp. 195–198, 2013.

Extra 1

Content of the .zip file

The .zip file is enclosed with the work, which contains:

- Root directory: contains the thesis in format pdf
- Directory **MATLAB_simulation**: contains scripts for implemented propagation models
- Directory **MATLAB_auxiliary**: contains auxiliary files for calculation and plotting the data
- Directory **Measured_data**: contains all the data outputs from spectrum analyzer and vector network analyzer